

1 Migration controls extinction and survival patterns of 2 foraminifers during the Permian-Triassic crisis in South China

3 Xiaokang Liu¹, Haijun Song^{1*}, David P.G. Bond², Jinnan Tong¹, Michael J. Benton³

4 ¹State Key Laboratory of Biogeology and Environmental Geology, School of Earth Sciences, China

5 University of Geosciences, Wuhan 430074, China

6 ²Department of Geography, Geology and Environment, University of Hull, Hull, HU6 7RX, UK

7 ³School of Earth Sciences, University of Bristol, Bristol, BS8 1RJ, UK

8 *Corresponding author. Email: haijunsong@cug.edu.cn

9 10 Abstract

11 The Permian-Triassic mass extinction, the greatest biotic crisis in Earth history, triggered the complete
12 replacement of ecosystems with the 5–10% surviving species giving rise to the Mesozoic fauna. Despite a
13 long history of systematic studies on Permian-Triassic foraminifera, there have been few investigations into
14 spatial and temporal patterns of survivorship and evolution during this critical interval. We interrogate a high-
15 resolution data set comprising newly obtained and previously published foraminiferal data (including 13,422
16 specimens in 173 species in 62 genera) from seven well-studied Permian-Triassic successions that record a
17 transect of platform to basin facies in South China. Shallow-water settings seen at the Cili and Dajiang
18 sections suffered a single-pulse, sudden extinction with high extinction rates at the end of the *Palaeofusulina*
19 *sinensis* Zone; deeper-water and slope environments seen at Liangfengya and Meishan experienced a two-
20 pulse extinction in the *Clarkina yini* and *Isarcicella staeschei* zones; basinal settings, seen at Shangsi, Gujiao

21 and Sidazhai, record a single, less devastating extinction pulse in and slightly above the *C. yini* Zone. In the
22 Late Permian, foraminiferal diversity was greatest on the shallow platforms, where 76.4% of species recorded
23 in our study lived. The two pulses of the Permian-Triassic extinction prompted this foraminiferal diversity
24 hotspot to move to deeper slope settings (comprising 75.6% of contemporary species) and finally basinal
25 settings (comprising 88.8% of species). We propose that foraminifera migrated to deeper water to avoid
26 overheating and toxicity in shallow waters that were driven by the emplacement of the Siberian Traps and
27 coeval volcanic activities around the Paleotethys Ocean. This study provides a methodological framework
28 for investigating survival mechanisms for foraminifers and other taxonomic groups during mass extinction
29 events.

30 **Keywords:** foraminifera; spatial-temporal evolution; selective extinction, survival strategy, deep-ward
31 migration

32 **1. Introduction**

33 It is estimated that four billion species have existed throughout Earth history and that 99% of these are
34 extinct (Novacek, 2001). Species naturally evolve and disappear, but the evolutionary balance of the planet
35 has also been interrupted by several major biotic crises (McGhee et al., 2013). The well-known “Big Five”
36 mass extinctions, and numerous lesser calamities, have pruned the branches of the tree of life over time,
37 enabling the survivors of these events and their descendants to establish new branches and shape life on Earth
38 as we know it. Thus, extinction survivors have played a fundamental role in the origins and macroevolution
39 of our biosphere. A key question remains: how and why could survivors survive mass extinctions? A variety
40 of survival strategies have been postulated for terrestrial animals, including poleward migration during times
41 of warming (Sun et al., 2012; Benton, 2018) and an ability to burrow (Waldrop, 1988; Robertson et al., 2004).

42 Thus, many mammalian survivors of the Cretaceous-Paleogene extinction are thought to have found refuge
43 in underground burrows, while non-avian dinosaurs (that could not burrow) suffered major losses ([Waldrop,](#)
44 [1988](#); [Robertson et al., 2004](#)). Fossil records show that tetrapods moved 10–15° poleward during the Permian-
45 Triassic extinction, probably in response to overheating in equatorial regions ([Sun et al., 2012](#); [Benton, 2018](#)).
46 Survival strategies in marine organisms are poorly understood, partly because of the difficulty in evaluating
47 detailed biological and ecological processes at the required spatial and temporal resolution through
48 geologically brief mass extinction period intervals.

49 The Permian-Triassic mass extinction (PTME) was the most devastating and ecologically severe of the
50 “Big Five” extinctions ([Alroy et al., 2008](#); [Song et al., 2018](#)), wiping out > 90% of marine species ([Erwin,](#)
51 [1994](#); [Song et al., 2013](#)) and resulting in the complete restructuring of life from Palaeozoic- to Mesozoic-
52 faunas ([Sepkoski, 1981](#)). The drivers of this mass extinction have been debated for half a century, and most
53 extinction scenarios invoke multiple climatic and environmental factors linked to the Siberian Traps large
54 igneous province ([Renne and Basu, 1995](#); [Burgess et al., 2017](#); [Shen et al., 2019](#); [Chu et al., 2020](#)) and coeval
55 volcanic activity around the Paleotethys Ocean ([Yin and Song, 2013](#)). Volcanically-derived stress factors
56 include global warming ([Joachimski et al., 2012](#); [Sun et al., 2012](#); [MacLeod et al., 2017](#)), anoxia ([Isozaki,](#)
57 [1997](#); [Grice et al., 2005](#); [Bond and Wignall, 2010](#); [Shen et al., 2016](#)) and ocean acidification ([Payne et al.,](#)
58 [2010](#); [Hinojosa et al., 2012](#); [Clarkson et al., 2015](#)).

59 The PTME was highly selective ([Knoll et al., 1996](#); [McKinney, 1997](#); [Clapham and Payne, 2011](#); [Song](#)
60 [et al., 2013](#)). Marine ecosystems shifted from dominance by non-motile animals to dominance by nektonic
61 organisms ([Song et al., 2018](#)), and non-motile animals suffered higher extinction magnitudes. Extinction
62 patterns and magnitudes among benthic organisms varied between shallow- and deep-water settings:

63 extinctions amongst foraminifers occur as a single pulse in platform sections (Groves et al., 2005; Song et
64 al., 2009b; Yang et al., 2016), but this group also suffered a second extinction pulse in slope settings (Song
65 et al., 2009a). In contrast, ostracods exhibit two extinction pulses in shallow settings, and while abundant
66 ostracods are found within the well-known Permian-Triassic microbialite unit, they disappear along with this
67 facies in the Griesbachian substage (lower Induan Stage) (Forel, 2013; Wan et al., 2019). In slope settings,
68 ostracods record only a single extinction pulse (Crasquin et al., 2010).

69 In exploring how survivors survived the PTME, Foraminifera have so far not been much considered.
70 The large fusulinacean foraminifera were among the dominant benthos in late Palaeozoic oceans until they
71 were eliminated during the PTME (Stanley and Yang, 1994). Smaller foraminifers also suffered severe loss
72 but a few species survived (perhaps due to their more efficient oxygen uptake) into the Triassic (Groves et
73 al., 2005; Payne et al., 2011). Foraminifers represent an excellent group to study the above questions because
74 they have a rich fossil record and they experienced the whole process of extinction, survival, and recovery
75 during the Palaeozoic-Mesozoic transition (Song et al., 2011b). They are one of the most common fossil
76 groups in Permian-Triassic marine strata due to their high abundance and the high preservation potential of
77 their calcified or agglutinated tests. They are, therefore, perfectly suited for high-precision quantitative
78 studies of the ecological strategies that facilitated survival during extinction events. Here, we use a detailed
79 record from South China to investigate survival strategies during the PTME interval, and hence to unpick the
80 underlying causes of the PTME.

81 There has been a long history of systematic studies on Permian-Triassic foraminifera from many regions,
82 including the Alps (Vachard and Miconnet, 1989; Groves et al., 2007; Nestell et al., 2011; Kolar-Jurkovšek
83 et al., 2013), Caucasia (Pronina, 1988; Vuks, 2000; Pronina-Nestell and Nestell, 2001; Vuks, 2007), Iran

84 (Kobayashi and Ishii, 2003; Aghai et al., 2009; Kolodka et al., 2012; Nejad et al., 2015), Japan (Kobayashi,
85 1997; Kobayashi, 2006; Kobayashi, 2012; Kobayashi, 2013), Tibet (Wang and Ueno, 2009; Wang et al., 2010;
86 Zhang et al., 2013; Zhang et al., 2016), Turkey (Altiner, 1981; Altiner et al., 2000; Altiner and Altiner, 2010;
87 Vachard and Moix, 2013), and South China (Gaillot et al., 2009; Song et al., 2009a; Song et al., 2011b; Song
88 et al., 2015). Earlier investigations have revealed that foraminiferal faunas from shallow to deep settings were
89 inconsistent in their response to the PTME (Gu et al., 2007; Song et al., 2009b; Zhang and Gu, 2015), thus it
90 is necessary to investigate their spatial evolution.

91 In this paper, we examine multiple facies in multiple localities to reveal the spatial-temporal evolution
92 of foraminifers during the PTME in South China. We perform a new quantitative analysis on seven sections
93 that record different facies and environments of deposition in South China, each of which has been previously
94 studied for its biostratigraphy, sedimentology, and geochemistry. This enables us to compare in detail, and
95 for the first time, how these key organisms responded to the mass extinction crisis in different oceanic settings.

96 **2. Key sections and stratigraphy**

97 During the Permian-Triassic boundary (PTB) interval, the South China Block was located in low latitude
98 eastern Paleotethys (Fig. 1B). The South China Block was a stable palaeogeographic unit from the Late
99 Proterozoic to the Middle Triassic and records diverse depositional lithofacies from shallow-water carbonates
100 to deep-water basin siliciclastics (Feng, 1997; Lehrmann et al., 1998; He et al., 2013). We have studied seven
101 sections that can be divided into three distinct sedimentary environments: shallow platform, slope, and basin
102 (Fig. 1 A and C). Specifically, shallow platform facies are recorded at Cili and Dajiang, and in the lower part
103 of the Liangfengya section (the Changxing Formation); slope facies are exposed at Meishan, in the upper
104 part of the Liangfengya section (the Feixianguan Formation), and the lower part of the Shangsi section (the

105 Dalong Formation); basal facies are seen in the upper part of the Shangsi section (the Feixianguan
106 Formation) and at Gujiao and Sidazhai. Each section preserves a continuous succession through the Permian-
107 Triassic transition apart from Sidazhai where the basal 7.9 m of the Luolou Formation are covered. The
108 sedimentary characteristics and biostratigraphic data for each section are discussed in detail below. We
109 divided the successions into three parts, i.e. late Changhsingian (*Clarkina yini* Zone), PTB interval (*C.*
110 *meishanensis* to *Isarcicella staeschei* zones), and the late Griesbachian. Strata in the PTB interval are
111 sometimes referred to as transitional beds (Yin and Wu, 1985) or mixed fauna beds (Teichert et al., 1970;
112 Sheng et al., 1984; Chen et al., 2005), characterized by mixed Permian-type and Triassic-type faunas.

113 2.1 Cili section

114 The Cili section, ~200 km west of Changsha city, Hunan Province, is located in the central part of the
115 Upper Yangtze carbonate platform (Feng et al., 1993) (Fig. 1B). The Permian-Triassic sequence is composed
116 of the Changxing and Daye Formations (Fig. 2). The late Changhsingian foraminifera *Palaeofusulina-*
117 *Colaniella* Zone occurs in the upper part of Changxing Formation (Wang et al., 2009). The first appearance
118 of *Hindeodus parvus* occurs at the base of the microbialite, i.e. lowest part of the Daye Formation (Wang et
119 al., 2016), and it has been suggested that there is a hiatus between the Changxing and Daye formations (Yin
120 et al., 2014). Wang et al. (2016) assign the beds above the microbialite to the *Isarcicella isarcica* Zone.

121 The Upper Permian Changxing Formation comprises 15 m of grey, thick-bedded bioclastic packstones
122 with an abundant and diverse fossil assemblage that includes fusulinids, small foraminifers, calcareous algae,
123 echinoderms, and *Tubiphytes* (Wang et al., 2009; Yang et al., 2013). Most of the bioclasts are well preserved,
124 but some fusulinids, echinoderms, and *Tubiphytes* were fragmented, suggesting that they were transported

125 from the edge of the reef area (Wang et al., 2009). The matrix is composed of micrite and rare calcisparite,
126 suggesting shallow back reef lagoon deposition with some turbulence (Wang et al., 1997; Wang et al., 2009).

127 The Lower Triassic Daye Formation, consisting of microbialites, oolitic limestones, vermicular
128 limestones, and limestones, has a sharp basal contact with the underlying bioclastic packstones. The lower
129 part of the Daye Formation yields a few fossil groups at low diversity, e.g. small foraminifers, small molluscs,
130 conodonts, and ostracods (Wang et al., 2009; Luo et al., 2013; Yang et al., 2013). The microbialite (Bed 2)
131 has similar petrographic features to the calcimicrobial framestone seen at Dajiang. Beds 3 and 4 at Cili are
132 oolitic limestone and vermicular limestone, respectively. The oolitic limestone is composed of well-preserved
133 grains. These grains are spherical or ellipsoidal with diameters between 0.2 mm and 0.6 mm, and are
134 surrounded by microspar and rarely, micrite (Wang et al., 2009). The development of microbialites and oolitic
135 limestones suggests shallow platform deposition (Wang et al., 1997; Wang et al., 2009).

136 2.2 Dajiang section

137 The Dajiang section, ~120 km south of Guiyang city, Guizhou Province, was deposited on the Great
138 Bank of Guizhou in the Nanpanjiang Basin, South China Block during the Late Permian period (Lehrmann
139 et al., 2003; Collin et al., 2009) (Fig. 1B). Its Permian-Triassic sequence consists of the Wujiaping and Daye
140 formations (Fig. 2). The late Changhsingian conodont *Clarkina changxingensis* is known from the upper part
141 of the Wujiaping Formation (Lehrmann et al., 2003). The first occurrence of the basal Triassic marker,
142 *Hindeodus parvus* is in the skeletal limestone that fills in hollows between the topmost Changxing Formation
143 and lowermost Daye Formation (Jiang et al., 2014). Accordingly, the microbialite is also assigned to the *H.*
144 *parvus* Zone (Lehrmann et al., 2003). The *Isarcicella lobata* and *Isarcicella isarcica* zones have been

145 identified in the overlying molluscan grainstone and limestones, respectively (Payne et al., 2004; Jiang et al.,
146 2014).

147 The Upper Permian Wujiaping Formation comprises 15 m of thick-bedded cherty skeletal packstone,
148 yielding diverse and abundant fossils, including fusulinids, sponges, rugose corals, crinoids, echinoid spines,
149 *Tubiphytes*, bivalves, gastropods and dasycladacean algae (Lehrmann et al., 2003; Song et al., 2009b). The
150 skeletal packstone contains abundant small fossil fragments whose cavities are filled with lime-mud,
151 suggesting deposition in a shallow platform environment near fair-weather wave base (Lehrmann et al., 2003).

152 The overlying Early Triassic Daye Formation comprises 16 m of massive-bedded calcimicrobial
153 framestone interbedded with molluscan lime grainstone, yielding only a few fossils, such as pectinacean
154 bivalves, small gastropods, small foraminifera, ostracods, rare echinoderms and brachiopods (Lehrmann,
155 1999; Lehrmann et al., 2003; Yang et al., 2011; Forel, 2012). The microbial fossils of the framework comprise
156 equant to lunate globular fossils with micrite walls that form irregular, tufted, and dendritic aggregates
157 (Lehrmann et al., 2003; Liu et al., 2007). The irregular intraframework cavities are several centimetres thick
158 and filled with micrite and other fossil fragments (Lehrmann et al., 2003; Lehrmann et al., 2015). These
159 microbial blooms and interlayered molluscan grainstones are characteristic of shallow marine subtidal
160 environments (Osleger and Read, 1991; Lehrmann, 1999; Lehrmann et al., 2003).

161 **2.3 Liangfengya section**

162 The Liangfengya section, ~13 km west of Chongqing city, was deposited in the west of the Upper
163 Yangtze platform during the Permian-Triassic transition (Fig. 1B). This section comprises the Changxing and
164 Feixianguan formations (Fig. 2). The late Changhsingian conodont *Clarkina changxingensis* was found in

165 the upper part of the Changxing Formation (Yuan and Shen, 2011). The Permian-Triassic boundary is
166 characterized by the first occurrence of *Hindeodus parvus* within a limestone (Bed 21c) in the uppermost
167 Changxing Formation (Peng and Tong, 1999; Yuan and Shen, 2011). The beginning of the late Griesbachian
168 is marked by the first occurrence of the ammonoid *Ophiceras* sp. (Wu, 1988).

169 The Upper Permian Changxing Formation (Beds 11 to 21) consists of 9.45 m of thick- to medium-
170 bedded bioclastic packstones with diverse fossils, including rugose corals, brachiopods, small foraminifers,
171 fusulinids, ostracods, calcareous algae, and conodonts (Yang et al., 1987; Tong and Kuang, 1990; Song et al.,
172 2011a). These abundant, well-preserved fossils are contained within micrite cements (some bioclasts are
173 micritised and abraded), suggesting that these sediments were deposited in an open platform (inter-reef)
174 setting with occasional perturbation (Tong and Kuang, 1990; Wignall and Hallam, 1996). The packstones are
175 interlayered with thin beds of clay that are up to a few centimeteres thick and consist entirely of illite and
176 montmorillonite (Wignall and Hallam, 1996).

177 The lower part of the Feixianguan Formation is characterized by thin- to medium-bedded marl
178 interbedded with black shale and yellowish clay (Bed 22). Bed 23 is characterized by alternations of yellow-
179 green laminar mudstone and calcareous mudstone, yielding a few bivalves, ammonoids, and brachiopods,
180 e.g. *Claraia grissbachi*, *C. hunanica*, and *Lingula* sp. (Yang et al., 1987). The marl is poorly bioturbated,
181 limited to small-sized burrows, and the abundance of small pyrite framboids in beds 16 to 22 suggests
182 oxygen-restricted conditions (Wignall and Hallam, 1996).

183 **2.4 Meishan section**

184 The Meishan section is located in Changxing County, Zhejiang Province (Fig. 1B), and is well known

185 as the Global Stratotype Section and Point (GSSP) for the Permian-Triassic boundary (Yin et al., 2001). The
186 Late Permian to Early Triassic succession is recorded by the Changxing and Yinkeng formations (Fig. 2).
187 The conodont biostratigraphy is well established (Yin et al., 2001; Jiang et al., 2007).

188 The upper Changxing Formation (Beds 19 to 24) is composed of 11.3 m of thick- to thin-bedded
189 bioclastic micrite and siliceous micrite, yielding diverse fossils, including foraminifers, sponge spicules,
190 crinoids, echinoids, brachiopods, bivalves, ostracods, microproblematica, and sporadically radiolarians (He
191 et al., 2005; Song et al., 2009a; Chen et al., 2015). Lithofacies and fossils indicate deposition in a low-energy
192 open slope environment still within the euphotic zone (Zhang et al., 1996; Cao and Zheng, 2007; Chen et al.,
193 2015).

194 The lowest part of the Yinkeng Formation is composed of marl and mudstone, interbedded with clays
195 with planar, fine lamination. The marls are mostly composed of micrite matrix with rare fragments of
196 foraminifers, ostracods, echinoids and brachiopods (Cao and Zheng, 2009; Chen et al., 2015). The lower part
197 of the Yinkeng Formation records a transgressive systems tract deposited beneath storm wave base (Zhang
198 et al., 1996). The middle to upper part of the Yinkeng Formation has been interpreted as having been
199 deposited in a relatively deep, offshore location (Chen et al., 2007; Chen et al., 2015). Pyrite framboid and
200 geochemical data suggest that depositional redox conditions became euxinic to dysoxic in the latest
201 Changhsingian (Beds 25-26a), and these persisted into the basal Triassic (Shen et al., 2011; Song et al., 2012;
202 Chen et al., 2015).

203 **2.5 Shangsi section**

204 The Shangsi section, ~230 km south of Chengdu city, Sichuan Province, was located in the Northern

205 Basin of the Yangtze Platform during the Permian-Triassic transition (Fig. 1A), and exposes the Dalong and
206 Feixianguan formations (Fig. 2). The biostratigraphic and cyclostratigraphic framework has been studied in
207 detail (Lai et al., 1996; Jiang et al., 2011; Wu et al., 2013; Yuan et al., 2019).

208 The upper part of the Dalong Formation comprises 2.98 m of thin-bedded dark grey, organic-rich micrite,
209 interbedded with claystone, yielding a deep-water fauna of ammonoids, radiolarians, conodonts, and small
210 foraminifers (Li et al., 1986; Wignall et al., 1995). Both the lithofacies and fossil groups suggest deposition
211 in an outer ramp to basinal facies (Jin, 1987; Wignall et al., 1995), somewhat deeper than Meishan.

212 The lowest part of the Feixianguan Formation (Bed 29) is composed of mudstone, marl, and claystone
213 with horizontal bedding, and includes sparse conodonts, bivalves, echinoids, and foraminifers. The remainder
214 of the lower Feixianguan Formation comprises thin- to thick-bedded marls and limestones interbedded with
215 mudstone, and contains rare Triassic fossils. The limestone is dominated by horizontal bedding and sporadic
216 cross bedding throughout the lower Feixianguan Formation, which suggests deposition within the reach of
217 storm waves in a lower carbonate ramp setting (Wignall et al., 1995; Xie et al., 2017).

218 **2.6 Gujiao section**

219 The Gujiao section, ~20 km southeast of Guiyang city, Guizhou Province, was located at the northern
220 margin of the Nanpanjiang Basin during the Permian-Triassic transition (Fig. 1B). The PTB sequence
221 comprises the Dalong and Daye Formations (Fig. 2), which are well exposed in this area. In our study, the
222 late Changhsingian index fossils *Pseudotirolites* sp. and *C. yini* were found in the lower part of the Dalong
223 Formation (Miao et al., 2019). The Permian-Triassic boundary marker, *H. parvus* occurs in the basal part of
224 the Daye Formation. The first occurrence of the Griesbachian ammonoid *Ophiceras medium* is in the

225 uppermost part of the Dalong Formation (Dai et al., 2018a; Dai et al., 2018b). We consider that the interval
226 from the top of the siliceous micrite to the first occurrence of *Ophiceras medium* constitutes the Permian
227 Triassic transitional beds.

228 The Dalong Formation comprises 11 m of thin-bedded micrite, siliceous micrite, dolomitized limestone,
229 and marl, interbedded with mudstone and claystone. These beds yield diverse ammonoids, nautiloids,
230 radiolarians, small foraminifers, sponge spicules, as well as transported brachiopods and bivalves (Zheng,
231 1981; Feng and Gu, 2002). The siliceous micrite is characterized by spherical or elliptical radiolarian
232 fragments surrounded by micrite, suggesting deposition in a basinal setting. The relative water depth of
233 Gujiao is inferred to have been deeper than at Shangsi based on the abundant open marine fossils and
234 development of anoxic conditions.

235 The lower Daye Formation consists of 6.6 m of thin-bedded marl and limestone interbedded with black
236 shale and mudstone. The marl contains a low abundance fossil assemblage of ammonoids, bivalves,
237 brachiopods, gastropods, foraminifers and ostracods (Dai et al., 2018a; Dai et al., 2018b).

238 **2.7 Sidazhai section**

239 The Sidazhai section, ~130 km south of Guiyang city, Guizhou Province, was located in the north of the
240 Nanpanjiang Basin during the Permian-Triassic transition (Fig. 1B). The Late Permian to Early Triassic
241 succession comprises the Linghao and Luolou Formations (Fig. 2). The conodont *Clarkina yini* has been
242 recovered from the base of the Linghao Formation (Ji, 2012), indicating a late Changhsingian age. The lower
243 part of the Luolou Formation yields ammonoids belonging to the *Ophiceras-Lytopiceras* assemblage (Huang,
244 2014), suggesting a late Griesbachian age.

245 The Linghao Formation comprises 13.4 m of medium- to thin-bedded limestone and siliceous limestone
246 interbedded with siliceous mudstone and yellow mudstone, yielding well-preserved fossils, including
247 foraminifers, radiolarians, ammonoids, brachiopods, bivalves, and conodonts (Ji, 2012; Huang, 2014). The
248 limestone (Bed 1) consists of a 4 m thick, grey, medium-bedded limestone with chert nodules and contains
249 pyrite framboids and diverse autochthonous fossil groups. The siliceous limestone (Bed 2) is characterized
250 by planar lamination, micrite fills with minor amounts of quartz, and deep-water fossil groups dominated by
251 radiolarians (e.g. *Latentifistula* sp., *Ormistonella* sp., and *Follicucullus* sp. (Feng et al., 2000; Gao et al.,
252 2001), sponge spicules, and small foraminifers. These sediments record deposition in a basinal setting. The
253 depth of Sidazhai is similar to that of Gujiao, but the former is more distal from the Yangtze platform.

254 The lower part of the Luolou Formation comprises 14.6 m of thin-bedded lutescent calcareous mudstone
255 interbedded with nodular limestones that yield a few bivalves, ammonoids, conodonts, and small foraminifers,
256 e.g. *Claraia griesbachi*, *Claraia orbicularis*, *Ophiceras* sp., and *Lytosphiceras* sp. (Ji, 2012; Huang, 2014;
257 Huang et al., 2018).

258 **3 Materials and methods**

259 We analyzed 13,422 individual foraminiferal specimens observed in 981 standard thin sections (2.2×2.2
260 cm²) from seven Permian-Triassic transitional sections in South China. Our new data from the Liangfengya,
261 Cili, Gujiao, Shangsi, and Sidazhai sections (see details in the Supplementary materials) is supported by data
262 from previously published records from Dajiang (Song et al., 2009b; Payne et al., 2011) and Meishan (Song
263 et al., 2009a). We construct a temporal framework for these sections using high-resolution biostratigraphic
264 correlations based on larger fusulinaceans, conodonts, and ammonoids. All newly obtained samples are
265 deposited in the School of Earth Sciences, China University of Geosciences, Wuhan, China.

266 **3.1 Cluster analysis**

267 Q-mode cluster analysis was performed using the paired group algorithm with the Euclidean distance
268 (or similarity) index ([Parker and Arnold, 2003](#); [Hammer and Harper, 2006](#); [Schröder-Adams et al., 2008](#)) to
269 examine the similarities of foraminiferal assemblages in our seven sections during the Late Permian-Early
270 Triassic interval. Our database comprises taxa at generic level and their relative abundances (as percentages)
271 in each section and each interval. We included 63, 23, and 21 genera for the late Changhsingian (*C. yini*
272 Zone), PTB interval, and the late Griesbachian intervals respectively. The cluster analyses were performed
273 with PAleontological STatistics (PAST), Version 3.16 ([Hammer et al., 2017](#)), using the unweighted paired
274 group method of arithmetic means with Euclidean similarity index to calculate the cluster trees. Foraminiferal
275 faunas with high similarity are aggregated on one tree primarily, with smaller distances between these.

276 **3.2 Confidence interval for estimating the extinction position**

277 The “last occurrences” of fossil taxa do not necessarily represent their true extinctions because of the
278 Signor-Lipps effect ([Meldahl, 1990](#); [Rampino and Adler, 1998](#)). This is especially the case for those species
279 that have less than 15% stratigraphic abundance (i.e. occurring in less than 15% of the sample intervals).
280 Statistical analyses can generate confidence levels (such as 50% or 95%; here we employ the 50% confidence
281 level) for the end of the stratigraphic range of a taxon. Confidence interval size depends inversely on the
282 sampling rate, based on the length of the stratigraphic range and the number of included fossil horizons. The
283 50% confidence interval, calculated from the binomial distribution ([Marshall, 1990](#); [Marshall and Ward, 1996](#))
284 and other improved methods ([Wang and Marshall, 2004](#); [Wang and Everson, 2007](#)) can predict the position
285 of the true extinction horizon with some certainty, and so we employ the 50% confidence interval method for
286 our four platform and slope sections. The confidence interval (r) is calculated according to [Strauss and Sadler](#)

287 (1989):

288
$$r = R[(1 - C)^{-1/(H-1)} - 1]$$

289 where C is confidence level, which in this case equals 50%, H is the number of fossil horizons, and R
290 is the observed stratigraphic range.

291 **3.3 Meldahl's method for testing the extinction pattern**

292 [Meldahl \(1990\)](#) developed a method with a “stratigraphic abundance vs. last occurrence” plot to negate
293 the Signor-Lipps effect, and test extinction patterns in the geological record. By modelling a sudden
294 extinction of a modern molluscan biota from the tidal zone in the northern Gulf of California, [Meldahl \(1990\)](#)
295 identified three extinction patterns, i.e. sudden, stepwise, and gradual. Sudden extinction exhibits an
296 accelerated diversity decline towards the extinction horizon. Stepwise extinction demonstrates a stepped
297 diversity decline. Gradual extinction appears as a constant decline ([Meldahl, 1990, figs 4–6](#)). Extinction
298 horizons for individual species are accurately recorded when their stratigraphic abundance is higher than
299 15%. Meldahl's (1990) method has been applied frequently to test extinction patterns based on stratigraphic
300 ranges in the marine fossil record ([Jin et al., 2000](#); [Groves et al., 2005](#); [Song et al., 2009b](#); [Angiolini et al.,](#)
301 [2010](#); [Jia and Song, 2018](#)). We employ Meldahl's (1990) method for our four platform and slope sections.

302 **3.4 Rarefaction analysis**

303 Sample- or individual-based rarefaction (species accumulation curve) is an interpolation method to
304 estimate how many species would be observed for any smaller or larger number of samples or individuals
305 ([Raup, 1975](#)). Our sample-based rarefaction follows the methods of [Colwell et al. \(2004\)](#), and individual-

306 based rarefaction follows the methods of [Colwell et al. \(2012\)](#). Rarefaction analyses were performed using
307 PAleontological STatistics (PAST), Version 3.16 ([Hammer et al., 2017](#)). For sample-based rarefaction, 739
308 samples were analyzed. Among these, the late Changhsingian data set includes 103 platform, 74 slope, and
309 55 basin samples; the PTB interval data includes 118 platform, 88 slope, and 50 basin samples; the late
310 Griesbachian data includes 45 platform, 94 slope, and 112 basin samples.

311 **4 Results**

312 Here, the systematic classification of the Order Lagenida follows [Groves et al. \(2003\)](#), while for other
313 orders we follow [Loeblich and Tappan \(1988\)](#) and [Loeblich and Tappan \(1992\)](#). In total, 173 species in 62
314 genera (plus additional unidentified elements, Table 1) belonging to five orders (Fusulinida, Lagenida,
315 Miliolida, Textulariida, and Involutinida) have been identified from the upper Changhsingian stage (*C. yini*
316 Zone) of the Late Permian and Griesbachian substage of the Early Triassic. These taxa are all characteristic
317 of the Late Permian to Early Triassic Paleotethys marine realm.

318 **4.1 Cili section**

319 We identified 1,511 specimens from 36 samples in the upper Changxing Formation. Seventy-two species
320 belonging to 34 genera (Fig. 3) are present in the *Palaeofusulina sinensis* fusulinacean Zone—this is an index
321 fossil zone for the late Changhsingian in South China ([Zhang and Yue, 2017](#)). Four species were identified
322 from 54 specimens in 38 samples from the *H. parvus* Zone. The fusulinacean assemblage comprises 238
323 specimens in 12 species of 4 genera (Table 1). A total of 326 specimens in 17 species of 10 genera are non-
324 fusulinacean fusulinids. The Order Lagenida is represented by 604 specimens in 32 species of 14 genera. The
325 most abundant genera are *Pachyphloia*, *Colaniella*, and *Nodosinelloide*. The Order Miliolida includes 326

326 specimens in 10 species of 5 genera, dominated by *Glomomidiellopsis*, *Hemigordius*, and *Glomomidiella*.
327 The textulariid *Ammodiscus* sp. is rarely observed in the upper Changxing Formation. During the extinction
328 pulse, all fusulinacean genera disappeared at the bioclastic packstone/microbialite boundary. The non-
329 fusulinacean fusulinids, *Diplosphaerina inaequalis*, and *Globivalvulina bulloides* occurred at the base of the
330 microbialite unit but then also vanished. *Postcladella kahlori* and *Earlandia* spp. are documented in younger
331 strata.

332 4.2 Dajiang section

333 Here we analyze the original foraminiferal data collected by [Song et al. \(2009b\)](#). A total of 615
334 specimens belonging to 60 species in 37 genera were determined from 34 thin sections from the late
335 Changhsingian *Palaeofusulina sinensis* foraminiferal Zone at Dajiang (Table 1). Five species of five genera
336 occur in the microbialite (in 37 samples). Three species were identified in the Griesbachian. The stratigraphic
337 ranges of these foraminifers are shown in Fig. 3 of [Song et al. \(2009b\)](#). Among these, the fusulinaceans
338 comprise 64 specimens in 7 species. Non-fusulinacean fusulinids are abundant and consist of 236 specimens
339 in 19 species and 13 genera. The Order Lagenida is represented by 176 specimens in 24 species and 12 genera.
340 The Order Miliolida is composed of 128 specimens in 7 species of 4 genera, of which *Glomomidiellopsis*
341 *tieni* ([Song et al. \(2009b\)](#)) reported as *Glomomidiella nestellorum*) and *Hemigordius* are the dominant taxa.
342 The Order Textulariida has the lowest abundance and diversity with only *Ammodiscus* sp. and *Glomospira*
343 spp. observed in the Changxing Formation. The Order Involutinida includes *Pseudovidalina* sp. with one
344 specimen and *Globivalvulina bulloides* and *Hemigordius longus* across the skeletal packstone-calcimicrobial
345 framestone boundary, which appear in the basal part of the microbialite, but disappear quickly. Three species,
346 *Postcladella kahlori*, *Earlandia* spp., and *Nodosaria expolita*, appear in the microbialite - gradually at first,

347 before the first two species become extraordinarily abundant in the earliest Triassic.

348 **4.3 Liangfengya section**

349 Thirty-four thin sections were examined from the *C. yini* Zone at Liangfengya, yielding 39 species in
350 21 genera (Fig. 4) amongst 279 specimens. A total of 418 specimens belonging to 16 species in 8 genera were
351 determined from 18 thin sections from the PTB interval (Table 1). Two species with 18 specimens were
352 collected from 18 samples in the *Ophiceras* sp. bed. The foraminiferal assemblage includes diverse lagenides,
353 which comprise 111 specimens in 22 species of 11 genera. The Order Fusulinida includes 165 specimens in
354 15 species of 8 genera. Of these, the fusulinaceans comprise 140 specimens in 10 species of 4 genera. Non-
355 fusulinacean fusulinids comprise 26 specimens in 5 species of 5 genera. *Glomomidiella nestellorum* is the
356 only representative of the Order Miliolida. After the first extinction pulse, 16 species survived the PTB
357 interval. The lagenides dominate this assemblage with 15 species. *Earlandia* spp. reaches extremely high
358 abundances in the limestone. Only *Nodosaria elabugae* and *Earlandia* spp. are recorded in the late
359 Griesbachian substage.

360 **4.4 Meishan section**

361 A total of 529 specimens from 47 thin sections have been identified from the *C. yini* Zone. The
362 foraminiferal assemblage includes 48 species in 28 genera (see Fig. 2 from [Song et al. \(2009a\)](#)). A total of 80
363 specimens belonging to 23 species in 16 genera (excluding an additional 12 unidentified species) were
364 determined from 70 thin sections from the PTB interval. Five species with 178 specimens were identified
365 from 39 samples in the late Griesbachian. Among these, 201 specimens in 24 species of 12 genera belong to
366 Lagenida. The fusulinaceans are represented only by *Reichelina* spp. The non-fusulinacean fusulinids include

367 181 specimens in 11 species of 12 genera. The Order Miliolida is represented by *Hemigordius* and
368 *Multidiscus* with ten species between them. The Order Textulariida includes *Ammovertella inversus* and
369 *Pseudoammodiscus parvus*. Lagenides become more dominant following the latest Permian extinction
370 (including eleven indeterminate species). *Tuberitina* sp. are the only representatives of the Order Fusulinida.
371 *Hemigordius* sp. A is also found in the PTB interval. The agglutinated tests of *Glomospira* spp. and
372 *Ammodiscus* sp., are recorded by single specimens. Above the level of the earliest Triassic extinction, the
373 Yinkeng Formation yields only five species. The disaster species *Earlandia* sp. appears with high abundance.

374 **4.5 Shangsi section**

375 A total of 27 thin sections were examined from the *C. yini* Zone at Shangsi, yielding 26 species in 19
376 genera (Fig. 5) amongst a total of 174 specimens. Eighteen species in 15 genera have been identified from
377 the PTB interval (from 46 samples). Griesbachian strata yielded 12 species in 9 genera from 86 samples. In
378 the *C. yini* Zone, 65 specimens in 14 species of 10 genera belong to Lagenida. The Order Fusulinida is
379 represented by 14 specimens in 3 species. The Order Miliolida includes 8 species in 5 genera. The Order
380 Textulariida includes *Glomospira* sp. During the PTB interval, the foraminiferal assemblage is relatively
381 diverse, and includes 18 species. Small and elongated lagenid elements dominate the assemblage. Fusulinida
382 and Miliolida include 2 and 4 species, respectively, in the PTB interval. Agglutinating foraminifera are
383 represented by *Ammodiscus* sp. and *Glomospira* sp., and these survive into the late Griesbachian. A total of
384 12 species from 353 specimens were collected in late Griesbachian strata (Table 1). Lagenida is represented
385 by 8 species. The Fusulinida and Miliolida are represented by *Earlandia* sp. and *Postcladella kahlori*,
386 respectively.

387 **4.6 Gujiao section**

388 Data from the Gujiao section come from the analysis of 52 thin sections. A total of 43 specimens,
389 including 13 species in 11 genera (Fig. 6) have been identified from the late Changhsingian. The Order
390 Lagenida dominates the foraminiferal assemblage at Gujiao and is represented by 33 specimens in 10 species
391 and 8 genera (Table 1). The Order Fusulinida is represented by *Earlandia* sp. The Order Miliolida is
392 represented by *Glomomidiella* sp. The Order Involutinida includes *Pseudovidalina* sp. Three specimens
393 belonging to *Nodosinelloides* spp. are documented from the PTB interval. Foraminifers rebound in late
394 Griesbachian strata and 149 specimens have been obtained from 19 thin sections. These belong to 11 species
395 in 11 genera (plus one additional indeterminate genus and species A). The Lagenida become increasingly
396 dominant both in abundance and taxonomic richness. The miliolids are represented only by *Planiinvoluta* sp.
397 and *Glomomidiella* sp. The Order Fusulinida is represented by *Earlandia* sp. and *Dagmarita* sp. A in the
398 Daye Formation. The most common agglutinated test in our samples is that of *Glomospira* sp., which occurs
399 in late Griesbachian strata.

400 **4.7 Sidazhai section**

401 A total of 143 specimens belonging to 16 species in 12 genera (Fig. 10) have been determined from 26
402 thin sections from the Linghao Formation. The Order Lagenida is represented by 132 specimens in 13 species
403 of 6 genera (Table 1). The non-fusulinacean fusulinids are represented by single occurrences of *Neoendothyra*
404 *parva* and *Dagmarita* sp. in the upper part of the limestone unit. Miliolida is represented by only two
405 specimens of *Glomomidiella* sp. and *Hemigordius qinglongensis*. Textulariides, including *Ammodiscus* sp.
406 and *Glomospira* spp. are observed. The lower part of the PTB interval in this section was covered. The upper
407 part of the PTB interval is represented by calcareous mudstone with no foraminifera present. Foraminifers
408 are seen again in limestones from the late Griesbachian. The assemblage is dominated by lagenides. Both

409 *Earlandia* sp. and *Ammodiscus* sp. are represented by single specimens in the lower part of the Luolou
410 Formation.

411 **5 Late Permian–Early Triassic foraminiferal fauna**

412 Three clusters (Fig. 8A–C) are identified from seven sections during the late Changhsingian, PTB
413 interval, and late Griesbachian. They are named after the dominant genera and species: A1. *Palaeofusulina-*
414 *Colaniella* assemblage; B1. *Hemigordius* assemblage; and C1. *Rectostipulina* assemblage in the late
415 Changhsingian (Fig. 8A); and A2. *Postcladella kalhori* assemblage; B2. *Geinitzina* assemblage; and C2.
416 undetermined (lack of specimens) from the PTB interval (Fig. 11B). These clusters appear to be depth-
417 controlled, and so we name them additionally as the A-platform assemblage, B-slope assemblage, and C-
418 basin assemblage, respectively. We did not identify the foraminiferal assemblages for the earliest Triassic
419 due to the paucity of preserved specimens.

420 **5.1 Late Changhsingian foraminiferal fauna**

421 A total of 143 species in 56 genera were determined from the late Changhsingian (*C. yini* Zone)
422 foraminiferal fauna. The Fusulinida dominate the platform assemblages with some larger taxa with complex
423 morphology, and then these decrease in abundance rapidly offshore, with some small fusulinids recorded in
424 slope areas and only a few elements found in basinal settings. The Lagenida dominate the slope and deeper
425 assemblages and comprise small and elongated infaunal elements. Their larger and more robust
426 representatives, such as *Pachyphloia* and *Colaniella*, preferred the shallow platform. The Miliolida is
427 represented by a few taxa on the platform, and some generalists spread into basin assemblages, whilst the
428 Textulariida is of low abundance and low diversity in all environments.

429 5.1.1 Platform settings

430 A platform foraminiferal assemblage (the *Palaeofusulina-Colaniella* assemblage) was identified from
431 Dajiang, Cili, and Liangfengya (Fig. 8A). A total of 110 species in 46 genera were identified. This assemblage
432 is characterized by the frequent occurrence of shallow-water taxa such as fusulinids, large lagenids, and
433 miliolids. Other ecological generalists occur with moderate abundance.

434 Large fusulinids had relatively low diversity but were still prevalent on the shallow seafloor.
435 *Palaeofusulina* and *Reichelina* are the most abundant fusulinids in the *Palaeofusulina-Colaniella* assemblage
436 in South China, and these taxa also flourish in other shallow platforms in the Caucasus, Thailand and Japan
437 (Sakagami and Hatta, 1982; Pronina-Nestell and Nestell, 2001; Kobayashi, 2006). *Palaeofusulina* and
438 *Reichelina* occur in varying quantities in platform assemblages (Fig. 9), probably having been transported
439 (Tong and Kuang, 1990; Lehrmann et al., 2003). Other large fusulinids like *Nankinella*, *Pisolina*, *Sphaerulina*,
440 and *Parareichelina* are rare or absent, and comprise no more than 3% (no more than three species) in the
441 platform assemblage. Fusulinaceans have a relatively large test and they demanded more food. They also had
442 specialized microhabitats (Brasier, 1995; Beavington-Penney and Racey, 2004) that were adaptations for
443 algal symbionts (Lee et al., 1979; Cowen, 1983; Lee and Hallock, 1987; Groves and Yue, 2009; Lee et al.,
444 2010; Forsey, 2013) due to their wall structure, ecology, facies distribution, and their evolutionary pattern.
445 Without exception, these taxa are mostly restricted to the shallow euphotic zone. Fusulinaceans also appear
446 to be susceptible to extinction driven by environmental change (Stanley and Yang, 1994; Yang et al., 2004;
447 Song et al., 2013). Shallow-water fusulinids such as *Palaeofusulina*, *Pisolina*, *Nankinella*, and *Sphaerulina*
448 produced ovate or fusiform tests with thick walls to prevent photoinhibition in bright sunlight and test damage
449 in turbulent water (Beavington-Penney and Racey, 2004). The genus *Reichelina* occurs in relatively deeper

450 habitats (Fig. 9), which might have been a response to competitive pressure and morphological adaptation
451 for endosymbiont advantage (Beavington-Penney and Racey, 2004).

452 The non-fusulinacean fusulinids are another important component of late Changhsingian assemblages,
453 mainly comprising members of superfamilies Biseriammininae and Palaeotextulariidae, with <10% of
454 occurrences in the platform assemblage. The Superfamily Palaeotextularoidea is very common in Paleotethys
455 and eastern Panthalassa (Lin et al., 1990; Kobayashi, 2006; Gaillot and Vachard, 2007; Vachard, 2016). The
456 Biseriammininae mainly includes *Globivalvulina*, *Dagmarita*, and *Paraglobivalvulina*, all of which preferred
457 shallow platform settings. Of these, the small subglobular tests *Dagmarita* are most common (up to 9.43%
458 of occurrences, Fig. 9) and with stable abundances in platform sections. *Globivalvulina* is found at moderate
459 abundance, ranging from 0.0% (Liangfengya) to 7.8% (Dajiang) of the total, and this genus is followed by
460 *Paraglobivalvulina* at less than 1%. The Palaeotextulariidae includes *Cribrogenerina*, *Climacammina*,
461 *Deckerella*, and *Palaeotextularia*. *Palaeotextularia* is the most prevalent genus in platform assemblages,
462 where it ranges from 0.26% to 5.37% of total abundance (Fig. 9). These are followed by *Cribrogenerina*,
463 *Deckerella*, and *Climacammina*, although the abundances of these decrease to zero at Liangfengya. Our
464 collections of Palaeotextulariidae are consistent with previous suggestions that they are mostly constrained
465 to settings above fair-weather wave base (e.g. in the Lower Carboniferous; Gallagher, 1998). They probably
466 had an epifaunal to shallow infaunal herbivorous lifestyle, and their strong and thick tabular tests protected
467 them from currents (Murray, 2006). The Superfamily Endothyracea includes *Postendothyra* and
468 *Neoendothyra*, found in higher quantities at Dajiang. However, these comprise less than 2.3% of the total
469 taxa, and they eventually disappear at Liangfengya. The primitive and small forms, such as *Diplosphaerina*
470 and *Earlandia* comprise low quantities but occur stably in platform sections (Fig. 9). Finally, some endemic
471 fusulinids, such as *Sengoerina* and *Tetrataxis*, are occasionally found in shallow platform assemblages.

472 The large lagenids, such as *Pachyphloia* (ranging from 3.14% to 10.39% of occurrences, Fig. 9) and
473 *Colaniella* (ranging from 0.72% to 8.07% of occurrences, Fig. 9) share a similar life strategy with the
474 elongated non-fusulinacean fusulinids (Insalaco et al., 2006; Zhang, 2015) and they are prevalent in shallow
475 sites, but not in deeper waters. They are characterized by thicker, stronger walls, which enable them to live
476 in shallow, turbulent environments. The small lagenids are dominated by *Nodosinelloides*, ranging from 5.76%
477 to 12.36% of the total in the *Palaeofusulina-Colaniella* assemblage. Some small lagenids are present at low,
478 but steady abundances in platform sections, such as *Geinitzina*, *Froncina*, *Ichthyofroncina*, and *Robuloides*
479 (< 4.66%, Fig. 9). Other elements, i.e. *Rectostipulina*, *Pseudolangella*, *Protonodosaria*, and *Cryptoseptida*,
480 occur sporadically and at low diversity in platform settings.

481 The Order Miliolida includes many opportunists and ecological generalists that normally occur in low
482 quantities, but proliferated rapidly when conditions were favorable (Kauffman and Harries, 1996; Groves
483 and Altiner, 2005). During the late Changhsingian interval, the large miliolids (such as taxa from families
484 Hemigordiopsidae and Neodiscidae) colonized and flourished in their preferred habitats on shallow carbonate
485 platforms (Fig. 9). The dominant miliolid in very shallow sections (Dajiang and Cili) is *Glomomidiellopsis*,
486 but it is absent at Liangfengya. *Glomomidiella* and *Hemigordius* are found at low abundances in platform
487 assemblages (1.08–4.07%). Genera like *Agathammina* and *Neodiscopsis* occur rather sporadically and are
488 restricted to shallow settings (Gaillot and Vachard, 2007; Gaillot et al., 2009). Most of the miliolids in this
489 study are coils of undivided tubular chambers and inflated to subspherical or discoid larger forms whose life
490 strategy was most likely surficial or epifaunal (Chan et al., 2017).

491 In contrast to other groups described here, the Textulariida constructed agglutinated tests. The
492 textulariides have one of the longest foraminiferal fossil records and inhabit the broadest range of habitats

493 from coast to deep ocean. The Order Textulariida has the lowest abundance and diversity in all our
494 assemblages. The agglutinated textulariides demonstrate ecological advantages in clastic facies (such as
495 clastic shelf and abyssal environments) when compared to carbonate facies (Armstrong et al., 2004; Murray,
496 2006). Their agglutinated tests are usually poorly preserved, and are difficult to identify (Hemleben et al.,
497 1990; Song et al., 2007). In our collections, *Glomospira* sp. and *Ammodiscus* sp. are present in platform
498 assemblages, but none of these comprises more than 2% of individuals (Fig. 9).

499 5.1.2 Slope settings

500 A slope foraminiferal assemblage (the *Hemigordius* assemblage) was identified at Meishan and Shangsi
501 (Fig. 9). A total of 63 species in 36 genera were identified in this assemblage, which is characterized by the
502 frequent occurrence of small lagenids, non-fusulinacean fusulinids, opportunistic miliolids, and a low
503 abundance of agglutinated tests.

504 The fusulinids are represented only by *Reichelina* spp., comprising 3.78% of the assemblages, and they
505 disappear at Shangsi. The non-fusulinacean fusulinids include 11 genera in the *Hemigordius* assemblage, but
506 only three genera, *Dagmarita*, *Globivalvulina*, and *Diplosphaerina*, recorded at both Meishan and Shangsi
507 (*Globivalvulina* is recorded in the PTB interval at Shangsi). The non-fusulinacean fusulinids are dominated
508 by Biseriammininae (mainly *Dagmarita*) and *Diplosphaerina* (11.30%). The lower limit of taxa, such as
509 *Palaeotextularia* and *Paraglobivalvulina* could not reach the depth in the Shangsi section. *Globivalvulina*
510 and *Paraglobivalvulina* are characterized by biserial with planispiral chambers strongly enveloping a
511 subglobular test. Their test structure suggests an epifaunal life position with mobility in turbulent eutrophic
512 environments (Setoyama et al., 2011; Zhang, 2015). With increasing water depth, the percentage of these
513 taxa falls, whilst the small lagenids become dominant. This pattern is also reported from other regions such

514 as Iran, as well as other sections in South China (Insalaco et al., 2006; Gu et al., 2007; Vachard et al., 2010;
515 Zhang and Gu, 2015). The lagenids are dominated by those with a small elongate test, such as
516 *Nodosinelloides*, comprising 20% of the fauna, followed by *Froncina* and *Geinitzina*. The larger lagenids
517 such as *Pachyphloia* and *Colaniella* occur at Meishan at less than 1% abundance. Other ecological generalists,
518 such as *Cryptoseptida*, *Rectostipulina*, and *Robuloides* are found in relatively low to moderate abundances
519 (< 4% of occurrences). The smaller discoidal test, *Hemigordius* flourishes in our slope assemblage, but rarely
520 occurs in the other assemblages. *Glomomidiella* is also found in this assemblage with high abundance at
521 Shangsi (Fig. 9) whilst *Multidiscus padangensis*, *Planinivoluta* sp., and ?*Meandrospira* sp. are occasionally
522 recorded in the *Hemigordius* assemblage, at < 5.8% abundance. The textulariides are represented by
523 *Pseudoammodiscus*, *Ammovertella*, and *Glomospira* but with low abundance and diversity.

524 5.1.3 Basinal settings

525 A basin foraminiferal assemblage (the *Rectostipulina* assemblage) was identified from Gujiao and
526 Sidazhai (Fig. 9) where a total of 29 species in 19 genera were identified. This assemblage is dominated by
527 small, elongate and flattened Lagenida, including *Nodosinelloides*, *Protonodosaria*, *Ichthyofroncina*, and
528 *Froncina* with total relative abundances up to 92% (at Sidazhai). The elongate tubular test *Rectostipulina* is
529 also important in this assemblage, and its abundance increases rapidly in basinal environments to 34% on
530 average. Most lagenids are generalists that could tolerate and spread into various environments (Murray,
531 2006; Gaillot and Vachard, 2007) but the small lagenids do not reach their maximum quantities within the
532 shallow environments; instead, they are most important in basinal settings. Other groups occur at low
533 diversity and abundance in the *Rectostipulina* assemblage. Within the Order Fusulinida, no large fusulinids
534 occur in the basinal assemblage. The non-fusulinacean fusulinids are represented by three species with

535 sporadic occurrences at Gujiao (including *Earlandia* sp.) and Sidazhai (including *Dagmarita* sp. and
536 *Neoendothyra parva*). The lifestyle of *Dagmarita* might have been epifaunal because the outer margins of its
537 chambers are joined with needle-like structures, which might have served to fasten the test to the sediment
538 surface. Aided by their life strategy and small tests, *Dagmarita* was able to tolerate basinal environments.
539 The lenticular and planispiral involute tests of *Robuloides* and *Neoendothyra* are not only similar to each
540 other in morphology, but also in spatial distribution. It is possible that they both developed a flattened
541 depressed planispiral form (with increased surface area to volume) as a strategy for living in or above shallow
542 sediments (Setoyama et al., 2011; Chan et al., 2017). The miliolids and textulariides are sporadically observed
543 at low diversity and abundance.

544 The planispiral involute test *Robuloides* occurs in low numbers in platform assemblages, reaching its
545 greatest abundance at Liangfengya, at 8.3%. Other taxa like *Langella*, *Nodosaria*, *Pseudolangella*, and
546 *Pseudoglandulina* (each < 1% abundance) are not strictly limited by lithofacies, but regularly occur in the
547 platform to basinal assemblages. Finally, some endemic lagenids, like *Pseudoglandulina*, *Cryptoseptida*,
548 *Calvezina*, and *Eocristellaria* are seen occasionally in various assemblages.

549 **5.2 PTB interval foraminiferal fauna**

550 Late Changhsingian foraminifera were major casualties of the latest Permian extinction, and the small
551 number of survivors, augmented by a few newcomers, make up the PTB interval foraminiferal fauna (Fig.
552 10). A total of 41 species in 23 genera were identified from this interval, and most of the survivors are seen
553 in slope settings. The Order Fusulinida includes five species in five genera in the microbialite and slope facies.
554 The Lagenida, which includes 28 species, dominates the slope and basinal environments with small elongated
555 infaunal taxa. The Miliolida is represented by five species, among which is the disaster taxon *Postcladella*

556 *kalhari*, which is very abundant in the microbialite. The Textulariida is represented by *Ammodiscus* sp. and
557 *Glomospira* sp. in slope and basinal facies.

558 **5.2.1 Platform settings**

559 The platform *Postcladella kalhari* foraminiferal assemblage is identified at Dajiang and Cili. The
560 eponymous species is one of the most common foraminiferal taxa to be found in the microbialite (Altiner et
561 al., 1980; Hips and Pelikán, 2002; Groves et al., 2005; Song et al., 2016). Foraminifers from this unit are
562 generally of low diversity and abundance, but some taxa occur sporadically at extremely high abundance –
563 the so-called disaster taxa (Song et al., 2016) that include *Postcladella kalhari*, *Globivalvulina bulloides* and
564 *Earlandia* spp. *Globivalvulina bulloides*, *Hemigordius longus* and *Diplosphaerina inaequalis* are found at
565 the base of the microbialite but disappear above that level. *Nodosaria expolita* (small lagenids) are also found
566 but with extremely low abundance and diversity in the *Postcladella kalhari* assemblage. No textulariides are
567 found in the microbialite, which indicates that microbial blooms may have provided unsuitable habitats for
568 agglutinated foraminifers.

569 **5.2.2 Slope settings**

570 The slope *Geinitzina* foraminifer assemblage was identified at Liangfengya and Meishan. During the
571 PTB interval, dominant taxa are elongate and flattened lagenid tests, with *Nodosinelloides* and *Geinitzina* as
572 the most abundant genera, at 40.43% and 17.7% of occurrences, respectively. *Nodosaria* and *Robuloides* are
573 found at moderate abundance in the *Geinitzina* assemblage. Other taxa, including *Amphoratheca*,
574 *Rectostipulina*, and *Fronidina* are also rarely found in the PTB interval. The Order Fusulinida is represented
575 by sporadically occurring *Diplosphaerina inaequalis*, *Globivalvulina bulloides*, *Neoendothyra* sp., and

576 *Tuberitina* sp. in the PTB interval but these vanish during the earliest Triassic extinction. *Earlandia* spp.
577 bloomed in slope settings, and this genus persists into the Triassic. *Ammodiscus* and *Glomospira* are also
578 seen at very low abundance and diversity at Meishan.

579 **5.2.3 Basin settings**

580 Basinal foraminiferal assemblages are recorded in the PTB interval at Shangsi and Gujiao. Shangsi has
581 a moderately abundant foraminiferal assemblage, whilst Gujiao yields only *Nodosinelloides* spp. No
582 foraminifera are found in this interval at Sidazhai. The assemblage at Shangsi is similar to the *Geinitzina*
583 assemblage, but with increased dominance of lagenids and miliolids. A few Lazarus taxa, such as *Tezaquina*
584 *clivuli* and *Planiinvoluta* sp. are seen at Shangsi where they occur in remarkable quantities in comparison to
585 the late Permian fauna.

586 **5.3 Late Griesbachian foraminiferal fauna**

587 The diversity of foraminifera decreased during the earliest Triassic extinction, and 26 species in 18
588 genera have been determined from late Griesbachian strata, most of which are known from basin settings.
589 The Order Fusulinida comprises two species, whilst the Lagenida includes 18 species that dominate basinal
590 environments with their small elongated and flattened tests (Fig. 11). The Miliolida is represented by four
591 species at low abundance. The Textulariida is represented by *Ammodiscus* sp. and *Glomospira* sp. in slope
592 and basinal settings.

593 **5.3.1 Platform settings**

594 Foraminifers occur in platform settings at extremely low diversity and abundance, and only three species

595 (*Earlandia* sp., *Postcladella kalhori*, and *Nodosaria expolita*) have been observed in our study. [Payne et al.](#)
596 (2011) reported three further species (*Postcladella grandis*, ?*Hoyenella* sp., and ?*Cornuspira ?mahajeri*) in
597 the Griesbachian substage, but the latter two had indeterminate identification and were represented by only
598 one specimen each.

599 **5.3.2 Slope settings**

600 Six species are found in the slope assemblage in the late Griesbachian. Of these, only *Earlandia* sp.
601 occurs with occasional high abundance at both Liangfengya and Meishan. The lagenids are represented by
602 *Nodosaria elabugae*, *Nodosinelloides aequiampla*, and *Lingulina* sp. with several specimens. The Order
603 Miliolida includes *Glomospira regularis* and *Glomospira* sp. B at Meishan.

604 **5.3.3 Basin settings**

605 The basin assemblage is more diverse than contemporaneous assemblages in shallower environments.
606 A total of 24 species in 17 genera have been identified, including *Earlandia* sp. and *Dagmarita* sp. A. The
607 Lagenida is represented by several relict genera (Fig. 11), such as *Nodosinelloides*, *Fronidina*, *Rectostipulina*,
608 and *Nodosaria* that dominate the earliest Triassic foraminiferal assemblages in abundance and diversity.
609 These taxa are characterized by small, uniserial flattened tests, which might have benefitted from gas
610 exchange in dysoxic to anoxic sediments due to their increased surface area to volume ratio ([Kaiho, 1994](#)).
611 The Miliolida is sporadically represented by *Postcladella kalhori*, *Glomomidiella* sp., and *Planiinvoluta* sp.
612 The Textulariida comprises *Glomospira* sp., *Ammodiscus* sp., which are found in low abundance.

613 **6 Extinction pattern**

614 It is well known that foraminifers suffered a catastrophic reduction in both diversity and abundance
615 during the PTME, not only in South China but globally (Tappan and Loeblich, 1988; Tong and Shi, 2000;
616 Groves and Altiner, 2005). The stratigraphic distributions of foraminifers from our study sections show
617 varying patterns of decline in the run-up to the PTB (Fig. 12). Here, we explore three distinct extinction
618 patterns in the foraminifera during the PTME.

619 **6.1 Single abrupt extinction pulse with a few survivors in platform settings**

620 The 50% confidence interval (red line, Fig. 3) method indicates a sudden extinction at Cili (a platform
621 setting) at the base of the microbialite. Using 50% confidence intervals, we show with dark stippling (Fig. 3)
622 in the microbialite interval that 26 species died out at the extinction horizon, and 23 species below.
623 Calculation of the binomial distribution of these 71 taxa (excluding 1, *Glomospira* sp.; 76, *Postcladella*
624 *kahlori*; 77, *Earlandia* sp. in Fig. 3) indicates with 99.7% probability that the extinction horizon lies within
625 the dark stippled area of Fig. 3, a 19.7 cm interval around the base of the microbialite (Marshall and Ward,
626 1996). Further, a total of 98.6% (71/72) of species disappeared in the PTB interval. Plots from Cili exhibit
627 hollow distribution curves consistent with a pattern of diversity decline in a simulation of sudden extinction
628 (Meldahl (1990), and 83.3% (60/72, Fig. 12A) of species disappear in the topmost 50 cm of the packstone.
629 The last occurrences of 31 of all 36 species (86.1%) with stratigraphic abundances > 15% disappear in the
630 same interval. *Globivalvulina bulloides* and *Diplosphaerina inaequalis* survived the main extinction pulse,
631 but these too eventually became extinct.

632 The same 50% confidence interval method also indicates that most species reach the extinction horizon
633 at Dajiang (platform). The predicted position of the true extinction horizon lies within a 62 cm interval that
634 includes skeletal packstone and the microbialite. Using the 50% confidence intervals method, foraminifers

635 show 17 species endpoints below and 16 species endpoints within the 62 cm dark stippling, suggesting there
636 was one sudden extinction, with a 97.1% probability that the extinction horizon lies within the predicted
637 range. A total of 93.3% (56/60) of taxa became extinct at Dajiang in the late Changhsingian. Although plots
638 of stratigraphic abundance versus last occurrence indicate that a few taxa started to disappear a few metres
639 below the PTB, a large number of species (51.9% of taxa, or 28/54, pink boxes in Fig. 12B) disappear in the
640 topmost 60 cm of packstone, in the latest Changhsingian. The last occurrences of 11 of all 13 species (84.6%)
641 with stratigraphic abundances > 15% disappear in the same interval (Song et al., 2009b), which also suggests
642 a sudden extinction. *Globivalvulina bulloides* and *Hemigordius longus* cross the packstone-microbialite
643 boundary and appear in the basal part of the microbialite unit, but they do not reappear in younger strata
644 (Song et al., 2009b).

645 To summarize, these two shallow platform sections suffered an abrupt extinction pulse (Fig. 13A), which
646 wiped out 98.6% and 93.3% of species at Cili and Dajiang, respectively. The abrupt extinction pattern
647 documented here has also been identified in other regions, such as Turkey (Groves et al., 2005), the southern
648 Alps (Groves et al., 2007), and northern Iran (Angiolini et al., 2010). The latest Permian extinction pulse was
649 so catastrophic that only six species are recorded in the microbialite unit and three of these disappeared
650 quickly. The earliest Triassic extinction pulse did not occur in foraminifers in platform settings. The
651 “microbialite refuge” idea (Forel, 2013; Foster et al., 2018; Foster et al., 2019) is that the shallow microbialite
652 environments were a shelter for some invertebrates, such as ostracods, bivalves, gastropods, and brachiopods.
653 But data from these two sections and some unpublished data (the Jianzishan, Shanggang, and Youping
654 sections in South China) indicate that shallow settings were unlikely to have been refuges for foraminifers.

655 **6.2 Two-pulse extinction in slope settings**

656 The grey contours in Figure 4 indicate the predicted position of the extinction horizon, assuming a two-
657 step decline at Liangfengya, which was located on the open platform to the upper slope (considering the
658 water depth in the Upper Yangtze platform) when the mass extinction occurred. The first predicted extinction
659 interval is located in a 16.8 cm thick interval between beds 17 and 19 (*C. yini* to *C. meishanensis* zones) with
660 92.9% probability (Fig. 4). Foraminifers show 50% confidence intervals for ten species endpoints below and
661 ten species endpoints within the first predicted extinction interval. Meanwhile, plots of stratigraphic
662 abundances versus last occurrences of taxa from Liangfengya indicate a sudden decline during the first pulse
663 that eliminated 47.7% of taxa (27/57, Fig. 12C) in bed 19 or slightly below this interval. The last occurrences
664 of all 15 species with stratigraphic abundances > 15% are in the same interval. The second predicted
665 extinction interval is between the top of beds 21a and 21b (7 cm interval) with 92.3% probability. The 50%
666 confidence-interval endpoints of the foraminifers include four species below and seven species within the
667 second contour. Fifteen out of 17 species (88.2%, pink boxes in Fig. 12C) disappear in the second extinction
668 pulse, including all nine species with stratigraphic abundances > 15%.

669 Data from the Meishan section (slope) confirm the hypothesis that there were two extinction levels, in
670 beds 25 and 28 (Song et al., 2009a, fig. 2), and this accords with stratigraphic abundance versus last
671 occurrence data (Fig. 12D). The 50% confidence interval method predicts that the extinction interval lies in
672 bed 25 at Meishan with 99.5% probability. The 50% confidence interval of last occurrences is bracketed by
673 14 species with endpoints above and 19 species with endpoints within the extinction interval. The first pulse
674 sees 76.6% of taxa (49/64) disappear within a 10 cm stratigraphic interval (i.e. uppermost 10 cm of Bed 24e)
675 or slightly below this interval (Song et al., 2009a) and 82.4% (14/17) of taxa with stratigraphic abundances >
676 15% disappear in this interval. The second predicted extinction interval lies between bed 28 and the lower
677 part of bed 29 with 81.1% probability, with eight species having 50% confidence-interval endpoints above

678 and seven endpoints within the secondary predicted extinction positional interval. The second pulse
679 eliminated 94.1% of taxa (32/34) in the 10 cm stratigraphic interval (i.e. the base of Bed 28), and eight species
680 with stratigraphic abundances > 15% disappear in this interval.

681 To sum up, both Liangfengya and Meishan show two extinction pulses (Fig. 13A), a pattern also seen
682 in southern Turkey, where the first pulse occurs at the base of oolitic limestones and the second pulse at the
683 base of a microbialite (Altiner, 2013). Liangfengya and Meishan exhibit similar extinction patterns, hinting
684 at shared processes (discussed below), with the first pulse eliminating taxa with large, complex morphologies,
685 and the second pulse chiefly affecting the small lagenids. The first extinction pulse was synchronous at
686 Liangfengya and Meishan, occurring at the top of the *C. yini* Zone. The second extinction pulse was possibly
687 also synchronous, although this is less certain. Thus, conodont biozones from Liangfengya include *C. yini*,
688 *C. meishanensis*, *H. preparvus*, and *H. parvus*. However, Yuan and Shen (2011) did not find conodonts from
689 beds 21b to 22, and placed this interval in the *H. preparvus* Zone. However, in another section at Daijiagou
690 ~50 km north of the Liangfengya section, *H. parvus* was found in the same interval (Yuan et al., 2015). So,
691 the second extinction pulse at Liangfengya is within (or a little above) the *H. parvus* Zone. Besides, Peng
692 and Tong (1999) claimed the claystone beds found at Liangfengya (bed 21b) and Meishan (bed 28) are
693 contemporaneous, which further suggests that the second extinction of foraminifers in these two sections is
694 synchronous.

695 **6.3 A single, less devastating extinction pulse in basin settings**

696 Data from basinal sections are insufficient for full evaluation of the precise levels of the extinction
697 horizons. However, one main extinction pulse of lower magnitude (when compared to shallow settings, Fig.
698 13A) can be identified in the *C. yini* Zone. The main extinction pulse eliminated 63.0% of taxa (17/27, Fig.

699 5), which gradually disappear between the *C. yini* and *C. meishanensis* zones at Shangsi. This main extinction
700 pulse corresponds to the extinction pulse in platform and the first pulse in slope settings. In addition, several
701 species gradually disappeared in the PTB interval, but it is difficult to pinpoint the second extinction pulse at
702 Shangsi. Similarly, Gujiao and Sidazhai also record the main extinction in the *C. yini* Zone (the first
703 occurrence of *C. yini* is below the main extinction interval) with 50% (9/18, Fig. 6) and 63.6% (14/22, Fig.
704 7) of taxa losses, respectively. In contrast to the platform area, 18 species are found in basinal strata from the
705 PTB interval. The basinal fauna is dominated by small lagenids and a few Lazarus taxa. The basinal fauna
706 did not suffer the second extinction pulse that occurred in slope settings. Additionally, diversity of the basinal
707 fauna rebounded moderately in the late Griesbachian.

708 These three distinct extinction patterns suggest that the three palaeoenvironmental settings we have
709 examined suffered different types and magnitudes of environmental fluctuations, and also different extinction
710 and survival processes. Shallow platform dwellers were impacted by high temperatures. Basinal taxa suffered
711 anoxia, whilst the mid water depths were influenced by both high temperatures and anoxia during the PTB
712 interval (Song et al., 2014). The environments recorded by the Cili and Dajiang sections quickly became
713 inhospitable. The deeper slope environments retained a habitable zone, and Liangfengya and Meishan shared
714 similar foraminiferal assemblages and water depths during the PTB interval. Basinal environments were
715 depauperate. As the temperature continued to rise (Fig. 14), the second extinction pulse occurred, forcing
716 survivors to migrate into basinal settings where they were able to tolerate the poor oxygen levels while
717 escaping from high temperatures (discussed below). Slope environments became uninhabitable for
718 foraminifers by the late Griesbachian.

719 **7 Selective extinction and survival**

720 Selective extinction of marine invertebrates during the PTME has been proposed several times (Knoll
721 et al., 1996; Clapham and Payne, 2011; Song et al., 2014) and was mostly a function of physiological
722 selectivity. Taxa that lacked physiological buffering and non-motile taxa suffered markedly higher extinction
723 rates (Knoll et al., 1996; Knoll et al., 2007). Similarly, taxa thought to be susceptible to anoxia and high
724 temperatures also suffered higher extinction magnitudes. It follows that the survival or extinction of a taxon
725 depends on how it was able to respond to these factors. The behaviours of foraminifera during the PTME
726 exhibit high selectivity in both taxonomy and ecology, and they are, therefore, an informative group for
727 evaluating different drivers of extinction.

728 **7.1 Taxonomic selectivity**

729 The Order Fusulinida experienced a severe extinction during the late Guadalupian (Capitanian, Middle
730 Permian) mass extinction, and never re-established their Middle Permian levels of diversity (Stanley and
731 Yang, 1994; Tong and Shi, 2000; Yang et al., 2004; Bond and Wignall, 2009). In the aftermath of that crisis,
732 non-fusulinacean fusulinids rapidly came to dominate Lopingian assemblages in low palaeolatitudinal
733 tropical shallow carbonate platform settings (Tong and Shi, 2000; Mohtat-Aghaï and Vachard, 2005;
734 Kobayashi, 2006; Gaillet and Vachard, 2007). During the latest Permian extinction pulse, fusulinids suffered
735 the greatest losses, and 92.3% of species became extinct (48/52, Fig. 13B). Those taxa with specialized
736 ecological distribution, large tests, and complex morphology all vanished, including all fusulinacean
737 fusulinids, all Palaeotextulariidae, and most Biseriamminidae (except *Globivalvulina bulloides*). In the PTB
738 interval, the non-fusulinacean fusulinids comprise primitive forms such as *Diplosphaerina inaequalis* and
739 *Earlandia* sp., and these are augmented by some moderately complex taxa such as *Globivalvulina bulloides*
740 and *Neoendothyra* sp. During the second extinction pulse, most non-fusulinacean fusulinids (except the

741 disaster taxon *Earlandia* sp.) disappeared.

742 The Lagenida originated in the Late Carboniferous (Tappan and Loeblich, 1988; Groves et al., 2003)
743 and underwent rapid expansion in inner to middle neritic environments throughout the Tethyan region and
744 northern higher palaeolatitudes after the late Guadalupian mass extinction (Groves and Altiner, 2005). Most
745 lagenids are generalists, which can tolerate and spread into various environments (Fig. 9). Among them, 63.3%
746 (38/60, Fig. 13B) vanished during the first extinction pulse. The large lagenids (such as *Pachyphloia* and
747 *Colaniella*) are characterized by thicker, stronger tests and these became extinct along with some other
748 robust-walled taxa. The lagenids were moderately diverse in slope settings during the PTB interval, and these
749 survivors are dominated by generalists with small flattened tests. The earliest Triassic extinction pulse
750 accounted for 62.1% of the diversity loss (18/29). The second pulse chiefly affected palmate-shaped taxa
751 such as *Geinitzina* and *Ichthyofrondina*, while the elongate and lanceolate tests such as *Nodosinelloides* and
752 *Nodosaria* became more dominant in the late Griesbachian.

753 Miliolids first appeared at the beginning of the Pennsylvanian (Late Carboniferous) and proliferated
754 rapidly in the Middle and Late Permian in Palaeotethys (Altiner et al., 2003; Jin and Yang, 2004). Miliolids
755 are mostly members of the Superfamily Cornuspiroidea in the Late Permian, and they suffered 84.6%
756 extinction (22/26) in the first extinction pulse. Miliolids include opportunists and some large, complex forms,
757 such as *Glomomidiellopsis*, *Agathammina*, *Neodiscus*, *Multidiscus*, and *Neodiscopsis*, all prominent victims
758 of the first pulse of extinction. Few miliolids survived into the PTB interval and these also suffered the second
759 extinction pulse. In the late Griesbachian, miliolids comprised only four Lazarus taxa or opportunists
760 (Kauffman and Harries, 1996). Textulariides are of low abundance and diversity in all our faunas and they
761 were only slightly affected by the PTME, while three species emerged again in the late Griesbachian. The

762 Involutinida includes one species, *Pseudovidalina* sp., which disappeared during the first extinction pulse.

763 **7.2 Selective extinction of shallow-water dwellers**

764 Here we divide foraminiferal species into two categories: shallow-water dwellers that are mainly seen
765 on the platforms but occasionally also appear in the slope facies, and widespread types that are commonly
766 seen in all three facies in the late Changhsingian. The shallow-water dwellers are mainly the fusulinids, large
767 lagenids, and miliolids. Widespread types include the small lagenids and some generalists from other groups.
768 There is a clear disparity in the extinction processes between these groups (Fig. 13C) because the shallow-
769 water dwellers suffered one abrupt extinction in the first pulse and with 96.7% of losses (58/60 species). The
770 single survivor, *Pseudolangella dorashamensis*, plus a new species, *Neoendothyra* sp., occur in slope settings
771 during the PTB interval, but these eventually became extinct in the second extinction pulse. In contrast, the
772 widespread elements lost 25% (4/16) and 33.3% (4/12) of diversity in the two extinction pulses, respectively.
773 The first extinction pulse wiped out moderately complex and robust taxa such as *Langella*, *Protonodosaria*,
774 and *Hemigordius*, and resulted in the contraction of habitats into the slope area. Shortly after this, widespread
775 types suffered the second extinction pulse, which saw the survivors remaining predominantly in deep basinal
776 environments.

777 **8 Deep-ward migration of foraminiferal diversity**

778 **8.1 Migration pattern**

779 In the late Changhsingian, the hotspot of foraminiferal diversity was concentrated in shallow platform
780 settings (Fig. 14) such as the Yangtze Platform and the Great Bank of Guizhou, where 110 species (76.4% of
781 the then extant fauna), including all 19 fusulinacean species, are found. Deeper-water environments also had

782 moderately diverse faunas in the late Changhsingian, with 63 (1 fusulinacean) and 29 (0 fusulinacean) species
783 found in slope and basinal settings, accounting for 43.8% and 20.1% of the total fauna (note, some species
784 exist in multiple settings). During the PTB interval, the diversity hotspot moved to the slopes, where 31
785 species (75.6% of the total fauna) were found. In contrast, platform (6 species) and basinal (18 species)
786 settings yield only a few foraminifers in the PTB interval. The diversity hotspot continued its migration to
787 deeper settings in the late Griesbachian, when basinal environments (24 species, 88.8% the total fauna)
788 became much more diverse than on the slopes (6 species) and platforms (3 species, Fig. 13).

789 Our data reveal that the selective extinction of shallow-water taxa partly accounts for the initial
790 migration of the diversity hotspot, as the disappearance of 58 shallow-water species caused a significant
791 decline in biodiversity on the platforms (Fig. 15A). Although widespread types also suffered severe losses
792 during the first pulse of extinction, over 30 species (including a few newcomers) are known from the PTB
793 interval. In contrast to the pre-extinction interval, the survivors of the first extinction pulse preferred slope
794 settings. By this time, shallow settings were occupied by a few disaster taxa, suggesting unfavourable
795 conditions for most species. Similarly, the deep basinal environments were also depauperate in foraminifers.
796 The transition of foraminiferal diversity hotspots from platform to slope settings may be explained in two
797 ways. First, as discussed above, the selectivity of extinction may have played an important role; although
798 shallow-water taxa apparently became “extinct” in those settings, some also lived in slope settings, where
799 they survived. Second, the survivors in slope settings also included taxa known from both pre-extinction
800 platform and basinal environments, suggesting that these taxa might have migrated to the slopes during
801 extinction, such as *Pseudolangella dorashamensis* and *Neoendothyra* sp. During the second extinction pulse,
802 the species (not recorded in basinal settings in the PTB interval) from the slope settings in the PTB interval
803 disappeared (or become extinct) in the late Griesbachian, whilst the survivors from the PTB interval (such as

804 *Fronndina permica*, *Geinitzina spandeli*, *Nodosaria skyphica*, *Nodosinelloides sagitta*, and *Rectostipulina*
805 *hexamerata*) and newcomers (such as *Nodosinelloides* sp. from Gujiao, *Fronndina* sp. from Sidazhai) are only
806 recorded in basinal settings in the late Griesbachian (Fig. 14). Ten species migrated from the slope settings
807 into basinal environments in the late Griesbachian. The second transition of foraminiferal diversity hotspots
808 was caused by the deep-ward migration of survivors of the second extinction pulse.

809 Subsample analysis shows that the decrease in biodiversity and the deep-ward migration of foraminifers
810 between the Late Permian and Early Triassic is not the result of sampling bias. Sample-based rarefaction was
811 performed on the late Changhsingian, PTB interval, and late Griesbachian data sets (Fig. 16). When the
812 randomly subsampled number reaches 200, the diversity patterns in our three sample intervals are revealed
813 to be complete. Sample-based rarefaction analysis was carried out for each facies within our three time bins
814 (Fig. 17). When the random subsampled size reaches 50 samples, it turns out that some settings were
815 insufficiently sampled, such as slope and basin settings in the late Changhsingian and the PTB interval.
816 Nevertheless, the diversity hotspot retains its pattern in being located on the platforms in the late
817 Changhsingian (100 species), on the slopes during the PTB interval (36 species), and in the basins during the
818 late Griesbachian (18 species). We also performed individual-based rarefaction to test for sampling bias, the
819 results of which further support our findings.

820 **8.2 Triggers of deep-ward migration**

821 Facies analysis suggests that sea-level change was not a key driver of the deep-ward migration of
822 foraminifers during the PTB interval. The sections record a marine regression, and this affected the
823 environment in the lower part of the PTB interval (equivalent to beds 25 to 27b at Meishan) in shallow
824 settings, such as Dajiang and Cili, but the deeper-water sections were not influenced. Strata representing the

825 upper part of the PTB interval (equivalent to beds 27c to 28 at Meishan) are well documented in these sections,
826 suggesting that sea level had risen by this time and re-established depositional environments similar to those
827 of the Late Permian. Nevertheless, during the second pulse of extinction, the survivors migrated to basinal
828 settings, which account for 88.8% of species.

829 The PTB mass extinction interval lasted ~30,000-60,000 years (Shen et al., 2018) and saw a ~10 °C rise
830 in sea surface temperatures in equatorial regions (Sun et al., 2012). Such extreme warming represents a
831 potentially potent driver of migration of foraminifers to deeper, cooler waters. Modern benthic foraminifers
832 are considered eurythermal as they are found in oceans from the tropics to the polar regions. The upper
833 thermal limit for most modern foraminifer species is usually <35 °C (Nigam et al., 2008; Song et al., 2014),
834 but experimental studies have demonstrated that the temperature range for reproduction is much narrower
835 than that for individual growth and survival (Nigam et al., 2008; Saraswat et al., 2011). Thus, *Rosalina*
836 *globularis* can survive temperatures from 20 °C to 35 °C, but reproduction only occurs at 25 °C (Saraswat et
837 al., 2011). Overheating of surface waters during the PTB interval and late Griesbachian may have rendered
838 them extremely unsuitable habitats for foraminifera. The survivors could have escaped the stress of high
839 temperatures by migrating either horizontally (latitudinally) or vertically. For marine animals, vertical
840 migration (if possible) is likely a more effective strategy than migration across the latitudes (Burrows et al.,
841 2019). Climate modelling suggests that water temperatures at 200–400 m depth were 10–14 °C cooler than
842 those in surface waters in equatorial regions during the PTB interval (Winguth et al., 2015). Deeper waters
843 may also have been a refuge for other animals as well as foraminifers, such as conodonts, bivalves, and
844 echinoids (Song et al., 2014; Godbold et al., 2017) during the crisis interval.

845 Toxic compounds released by the Siberian Traps large igneous province and minor volcanic activities

846 around the Palaeotethys Ocean (Yin and Song, 2013; Burgess et al., 2017) (Fig. 14) are a further potential
847 driver of foraminiferal migration. The Siberian Traps in particular released vast quantities of toxic
848 compounds, including poisonous metals (Sanei et al., 2012), noxious gases (Keller and Kerr, 2014) and chars
849 (Grasby et al., 2011), which might have transformed surface seawaters into a toxic soup in which foraminifers
850 could barely survive. This would have been compounded by additional loading of potentially toxic products
851 from massive soil erosion and/or biomass burning. In contrast, deeper waters were likely less affected by
852 these products of volcanism. The harmful effects of these toxic compounds were probably “consumed” by
853 those organisms that persisted in shallow waters (Grasby et al., 2017; Shen et al., 2019). A modern analogy
854 for our scenario is Sorfjord in western Norway – one of the most metal-polluted fjords in the world – where
855 benthic foraminifers have transferred their habitat to deeper waters just within their tolerance limits to escape
856 toxicity in surface waters (Alve, 1991).

857 A great body of evidence supports the development of intense marine anoxia in both deep and shallow
858 waters (within the photic zone) during the PTME interval (Wignall and Twitchett, 1996; Grice et al., 2005;
859 Algeo et al., 2010). A major increase in the $\delta^{13}\text{C}$ -depth gradient after the PTME suggests that deeper waters
860 experienced more intense and prolonged oxygen restriction (Meyer et al., 2011). Observations on living
861 foraminifers provide some clues about how they might have survived in low-oxygen conditions. Laboratory
862 experiments show that the oxygen consumption rate increases significantly in foraminiferal specimens larger
863 than 250 μm (Bradshaw, 1961), and we note that many of the surviving taxa were small (mostly < 200 μm).
864 Furthermore, the elongate-tapered tests of survivors such as *Nodosinelloides*, *Nodosaria*, and *Geinitzina*
865 possess higher surface area-to-volume ratios that likely improved mitochondrial oxygen uptake (Kaiho,
866 1994). It is also notable that many living foraminifers are capable of (even complete) denitrification (by using
867 NO_3^- for respiration rather than oxygen) enabling them to flourish in the oxygen minimum zone (Risgaard-

868 [Petersen et al., 2006](#)). Culture experiments show that denitrification is an auxiliary metabolic mechanism for
869 cell maintenance in many foraminiferal groups, including Lagenida, Miliolida, Textulariida, and Rotaliida
870 ([Piña-Ochoa et al., 2010](#)). Further, denitrification has been shown to be a more efficient metabolism than
871 aerobic respiration in some benthic foraminifers in the Peruvian oxygen minimum zone, and the ability of
872 oxygen respiration still remains ([Glock et al., 2019](#)). Previous evidence indicates that intensive denitrification
873 and/or anaerobic ammonium oxidation occurred during the PTME, and the foraminifera may play an
874 important role in denitrification ([Sun et al., 2019](#)). It has been suggested that modern benthic foraminifera
875 are responsible for up to 70 % of the total denitrification in several regions ([Piña-Ochoa et al., 2010](#); [Glock](#)
876 [et al., 2013](#)). Enhanced nitrogen fixation by cyanobacteria and other microbes has been suggested for the
877 PTME ([Luo et al., 2011](#)), which may have continuously supplied nitrates to the anoxic water masses.
878 Foraminifers living within the oxygen minimum zone, such as rotaliids, are able to store extremely high
879 concentrations of nitrate seawater (several hundred times that of pore water) in large vacuoles for
880 denitrification ([Bernhard et al., 2012](#)). Phylogenetic reconstruction of the enzymes' evolutionary history
881 suggests an ancient acquisition of the foraminiferal denitrification pathway from prokaryote ancestors in the
882 early Phanerozoic ([Woehle et al., 2018](#)). The evolution of hybrid respiration in foraminifera likely contributed
883 to their ecological success in surviving during times of oxygen restriction and biotic crises such as the PTME.

884 Foraminifera have a higher tolerance of low oxygen levels than most other marine taxa ([Song et al.,](#)
885 [2014](#)). Other hypoxia-tolerant groups include bivalves, gastropods, cephalopods, and corals, with bryozoans,
886 echinoderms, ostracods, and non-ostracod crustaceans being much less tolerant. Predictions of survivorship,
887 however, depend on complex interactions between oxygen level and temperature, with oxygen requirements
888 of most animals increasing with temperature ([Pörtner, 2010](#)). However, the oxygen solubility of the seawater
889 declined while temperatures rose during the PTME. Therefore, the oxygen requirement might be less in a

890 cool water environment than a hot environment, and this might have been important for some taxa. Warming
891 of the modern oceans and consequent loss of dissolved oxygen are reshaping the biogeography of some fishes
892 and arthropods, forcing them to contract their ranges in the last few decades both vertically and poleward to
893 occupy metabolically viable habitats (Deutsch et al., 2015). The vulnerability of marine organisms to hypoxia
894 may cause them to migrate or even become extinct before reaching the temperature threshold (Pörtner and
895 Knust, 2007). Physiological and ecological simulations of the PTME show that organisms with higher
896 temperature sensitivity (some taxa among arthropods and chordates) may have vacated habitats in shallow
897 areas at low latitudes (Penn et al., 2018). Physiological evidence suggests that some invertebrates, such as
898 sipunculids, annelids or bivalves, possess an alternative mitochondrial oxidase in aerobic respiration
899 (Buchner et al., 2001). The alternative oxidase may represent an ancient mechanism to tolerate oxygen-poor
900 environments, and this is still prevalent in some invertebrates in hypoxic environments (Pörtner, 2010).
901 Notably, taxa with high temperature tolerances, such as ostracods and gastropods, were able to survive in the
902 shallow waters in the earliest Triassic, and these are major components of the microbialite.

903 **Conclusion**

904 A total of 13,422 individual foraminiferal specimens belonging to 173 species in 62 genera have been
905 analyzed from seven different paleoenvironmental settings across the Permian-Triassic boundary in South
906 China. Three foraminiferal faunas, from the late Changhsingian, the Permian-Triassic boundary interval, and
907 the late Griesbachian, were identified, and these are separated by two pulses of the PTME. These three faunas
908 reveal that the foraminiferal diversity hotspot moved from shallow platforms to deeper slopes and finally into
909 basinal settings during the PTME within ~30,000-60,000 years. Quantitative analysis presents three
910 extinction patterns: 1) shallow sections exhibit one abrupt extinction pulse with 97.3% of species lost; 2)

911 slope settings experienced two stepwise extinction pulses, in which 63.5% and 90.5% of total taxa became
912 extinct; 3) basin dwellers suffered one main extinction pulse in which > 50% of species were lost. The
913 selective extinction of foraminifers reveals that both large and complex-morphology taxa (such as fusulinids)
914 and shallow water dwellers were prominent victims of the first extinction pulse. We suggest that the deep-
915 ward shift in diversity was a strategy to avoid overheated and toxic shallow waters that resulted from intense
916 volcanic activity in the Siberian Traps and coeval volcanism around the Palaeotethys Ocean. This ecological
917 strategy for escaping the deadly drivers of extinction may provide a key to understanding how some marine
918 species survived this catastrophic crisis and how modern ocean dwellers might escape warming oceans in the
919 coming decades.

920 **Acknowledgements**

921 We thank Xu Dai and Enhao Jia for their help in the field, Ruoyu Bai for conodont biostratigraphy, and
922 Lirong Yang for identification of foraminifera. This study is supported by the National Natural Science
923 Foundation of China (41821001, 41622207, 41530104, and 41661134047), the State Key R&D Project of
924 China (2016YFA0601100), the Strategic Priority Research Program of Chinese Academy of Sciences (No.
925 XDB26000000), and the UK Natural Environment Research Council's Eco-PT project (NE/P01377224/1)
926 and Advanced Research Fellowship (NE/J01799X/1). This study is a contribution to the IGCP 630 project.

927 **References**

928 Aghai, P.M., Vachard, D. and Krainer, K., 2009. Transported foraminifera in Palaeozoic deep red nodular
929 limestones exemplified by latest Permian Neoendothyra in the Zal section (Julfa area, NW Iran). *Revista*
930 *española de micropaleontología*, 41(1–2): 197–213.

931 Algeo, T.J., Hinnov, L., Moser, J., Maynard, J.B., Elswick, E., Kuwahara, K. and Sano, H., 2010. Changes in
932 productivity and redox conditions in the Panthalassic Ocean during the latest Permian. *Geology*, 38(2):
933 187–190.

934 Alroy, J., Aberhan, M., Bottjer, D.J., Foote, M., Fürsich, F.T., Harries, P.J., Hendy, A.J., Holland, S.M., Ivany, L.C.
935 and Kiessling, W., 2008. Phanerozoic trends in the global diversity of marine invertebrates. *Science*,
936 321(5885): 97–100.

937 Altiner, D., 1981. Le Trias dans la region de Pinarbasi, Taurus oriental, Turki: unites lithologiques,
938 micropaleontologie, milieux de depot. *Rivista Italiana di Paleontologia e Stratigrafia*, 86(4): 705–738.

939 Altiner, D., 2013. Evolutionary changes in Changsingian foraminifera: extinction and post-extinction recovery.
940 *Acta Geologica Sinca*, 87(supp): 897–899.

941 Altiner, D. and Altiner, S.Ö., 2010. *Danielita gailoti* n. gen., n. sp., within the evolutionary framework of Middle-
942 Late Permian dagmaritins. *Turkish Journal of Earth Sciences*, 19(4): 497–512.

943 Altiner, D., Baud, A., Guex, J. and Stampfli, G., 1980. La limite Permien-Trias dans quelques localités do Moyen-
944 Orient: Recherches stratigraphiques et micropaléontologique. *Rivista Italiana di Paleontologia*, 85: 683–
945 714.

946 Altiner, D., Özkan-Altiner, S. and Koçyiğit, A., 2000. Late Permian foraminiferal biofacies belts in Turkey:
947 palaeogeographic and tectonic implications. *Geological Society, London, Special Publications*, 173(1):
948 83–96.

949 Altiner, D., Savini, R. and Özkan-Altiner, S., 2003. Morphological variation in *hemigordius harltoni* Cushman &
950 Waters, 1928: remarks on the taxonomy of Carboniferous and Permian hemigordiopsids. *Rivista Italiana*
951 *di Paleontologia e Stratigrafia*, 109(2): 195–211.

952 Alve, E., 1991. Benthic foraminifera in sediment cores reflecting heavy metal pollution in Sorfjord, western

- 953 Norway. *Journal of Foraminiferal Research*, 21(1): 1–19.
- 954 Angiolini, L., Checconi, A., Gaetani, M. and Rettori, R., 2010. The latest Permian mass extinction in the Alborz
955 Mountains (north Iran). *Geological Journal*, 45(2–3): 216–229.
- 956 Armstrong, H.A., Brasier, M.D., Armstrong, H.A. and Brasier, M.D., 2004. *Foraminifera, Microfossils*. Blackwell
957 Publishing, pp. 142–187.
- 958 Beavington-Penney, S.J. and Racey, A., 2004. Ecology of extant nummulitids and other larger benthic foraminifera:
959 applications in palaeoenvironmental analysis. *Earth Science Reviews*, 67(3): 219–265.
- 960 Benton, M.J., 2018. Hyperthermal-driven mass extinctions: killing models during the Permian–Triassic mass
961 extinction. *Philosophical Transactions of the Royal Society A: Mathematical, Physical and Engineering
962 Sciences*, 376(2130): 20170076.
- 963 Bernhard, J.M., Edgcomb, V.P., Casciotti, K.L., McIlvin, M.R. and Beaudoin, D.J., 2012. Denitrification likely
964 catalyzed by endobionts in an allogromiid foraminifer. *The ISME journal*, 6(5): 951–960.
- 965 Bond, D.P.G. and Wignall, P.B., 2009. Latitudinal selectivity of foraminifer extinctions during the late Guadalupian
966 crisis. *Paleobiology*, 35(4): 465–483.
- 967 Bond, D.P.G. and Wignall, P.B., 2010. Pyrite framboid study of marine Permian-Triassic boundary sections: A
968 complex anoxic event and its relationship to contemporaneous mass extinction. *Geological Society of
969 America Bulletin*, 122(7–8): 1265–1279.
- 970 Bradshaw, J.S., 1961. Laboratory experiments on the ecology of foraminifera. *Cushman Foundation for
971 Foraminiferal Research Contributions* 17: 87–106.
- 972 Brasier, M.D., 1995. Fossil indicators of nutrient levels. 2: Evolution and extinction in relation to oligotrophy.
973 *Geological Society of London Special Publications*, 83(1): 133–150.
- 974 Buchner, T., Abele, D. and Pörtner, H.-O., 2001. Oxyconformity in the intertidal worm *Sipunculus nudus*: the

975 mitochondrial background and energetic consequences. *Comparative Biochemistry and Physiology Part*
976 *B: Biochemistry and Molecular Biology*, 129(1): 109–120.

977 Burgess, S.D., Muirhead, J.D. and Bowring, S.A., 2017. Initial pulse of Siberian Traps sills as the trigger of the
978 end-Permian mass extinction. *Nature Communications*, 8(1): 164.

979 Burrows, M.T., Bates, A.E., Costello, M.J., Edwards, M., Edgar, G.J., Fox, C.J., Halpern, B.S., Hiddink, J.G.,
980 Pinsky, M.L., Batt, R.D., García Molinos, J., Payne, B.L., Schoeman, D.S., Stuart-Smith, R.D. and
981 Poloczanska, E.S., 2019. Ocean community warming responses explained by thermal affinities and
982 temperature gradients. *Nature Climate Change*, 9(12): 959–963.

983 Cao, C. and Zheng, Q., 2007. High-resolution lithostratigraphy of the Changhsingian stage in Meishan section D,
984 Zhejiang. *Journal of Stratigraphy*, 31: 14–22.

985 Cao, C. and Zheng, Q., 2009. Geological event sequences of the Permian-Triassic transition recorded in the
986 microfacies in Meishan section. *Science in China Series D: Earth Sciences*, 52(10): 1529–1536.

987 Chan, S.A., Kaminski, M.A., Al-Ramadan, K. and Babalola, L.O., 2017. Foraminiferal biofacies and depositional
988 environments of the Burdigalian mixed carbonate and siliciclastic Dam Formation, Al-Lidam area,
989 Eastern Province of Saudi Arabia. *Palaeogeography, Palaeoclimatology, Palaeoecology*, 469: 122–137.

990 Chen, Z., Tong, J., Kaiho, K. and Kawahata, H., 2007. Onset of biotic and environmental recovery from the end-
991 Permian mass extinction within 1–2 million years: a case study of the Lower Triassic of the Meishan
992 section, South China. *Palaeogeography, Palaeoclimatology, Palaeoecology*, 252(1–2): 176–187.

993 Chen, Z.Q., Kaiho, K. and George, A.D., 2005. Survival strategies of brachiopod faunas from the end-Permian
994 mass extinction. *Palaeogeography, Palaeoclimatology, Palaeoecology*, 224(1–3): 232–269.

995 Chen, Z.Q., Yang, H., Luo, M., Benton, M.J., Kaiho, K., Zhao, L., Huang, Y., Zhang, K., Fang, Y. and Jiang, H.,
996 2015. Complete biotic and sedimentary records of the Permian–Triassic transition from Meishan section,

997 South China: Ecologically assessing mass extinction and its aftermath. *Earth-Science Reviews*, 149: 67–
998 107.

999 Chu, D., Grasby, S.E., Song, H., Dal Corso, J., Wang, Y., Mather, T.A., Wu, Y., Song, H., Shu, W. and Tong, J.,
1000 2020. Ecological disturbance in tropical peatlands prior to marine Permian-Triassic mass extinction.
1001 *Geology*.

1002 Clapham, M.E. and Payne, J.L., 2011. Acidification, anoxia, and extinction: A multiple logistic regression analysis
1003 of extinction selectivity during the Middle and Late Permian. *Geology*, 39(11): 1059–1062.

1004 Clarkson, M., Kasemann, S., Wood, R., Lenton, T., Daines, S., Richoz, S., Ohnemueeller, F., Meixner, A., Poulton,
1005 S. and Tipper, E., 2015. Ocean acidification and the Permo-Triassic mass extinction. *Science*, 348(6231):
1006 229–232.

1007 Collin, P.Y., Kershaw, S., Crasquin - Soleau, S. and Feng, Q., 2009. Facies changes and diagenetic processes
1008 across the Permian–Triassic boundary event horizon, Great Bank of Guizhou, South China: a controversy
1009 of erosion and dissolution. *Sedimentology*, 56(3): 677–693.

1010 Colwell, R.K., Chao, A., Gotelli, N.J., Lin, S.-Y., Mao, C.X., Chazdon, R.L. and Longino, J.T., 2012. Models and
1011 estimators linking individual-based and sample-based rarefaction, extrapolation and comparison of
1012 assemblages. *Journal of Plant Ecology*, 5(1): 3–21.

1013 Colwell, R.K., Mao, C.X. and Chang, J., 2004. Interpolating, extrapolating, and comparing incidence - based
1014 species accumulation curves. *Ecology*, 85(10): 2717–2727.

1015 Cowen, R., 1983. Algal Symbiosis and Its Recognition in the Fossil Record. In: M.J.S. Tevesz and P.L. McCall
1016 (Editors), *Biotic Interactions in Recent and Fossil Benthic Communities*. Springer US, Boston, MA, pp.
1017 431–478.

1018 Crasquin, S., Forel, M.-B., Qinglai, F., Aihua, Y., Baudin, F. and Collin, P.-Y., 2010. Ostracods (Crustacea) through

- 1019 the Permian-Triassic boundary in South China: the Meishan stratotype (Zhejiang Province). *Journal of*
1020 *Systematic Palaeontology*, 8(3): 331–370.
- 1021 Dai, X., Song, H., Brayard, A. and Ware, D., 2018a. A new Griesbachian–Dienerian (Induan, Early Triassic)
1022 ammonoid fauna from Gujiao, South China. *Journal of Paleontology*, 93(1): 48–71.
- 1023 Dai, X., Song, H., Wignall, P.B., Jia, E., Bai, R., Wang, F., Chen, J. and Tian, L., 2018b. Rapid biotic rebound
1024 during the late Griesbachian indicates heterogeneous recovery patterns after the Permian-Triassic mass
1025 extinction. *GSA Bulletin*, 130(11–12): 2015–2030.
- 1026 Deutsch, C., Ferrel, A., Seibel, B., Pörtner, H.-O. and Huey, R.B., 2015. Climate change tightens a metabolic
1027 constraint on marine habitats. *Science*, 348(6239): 1132–1135.
- 1028 Erwin, D.H., 1994. The Permo–Triassic extinction. *Nature*, 367(6460): 231–236.
- 1029 Feng, Q. and Gu, S., 2002. Uppermost Changxingian (Permian) Radiolarian fauna from Southern Guizhou,
1030 Southwestern China. *Journal of Paleontology*, 76(5): 797–809.
- 1031 Feng, Q., Yang, F., Zhang, Z., Zhang, N., Gao, Y. and Wang, Z., 2000. Radiolarian evolution during the Permian
1032 and Triassic transition in South and Southwest China. *Developments in Palaeontology & Stratigraphy*,
1033 18: 309–326.
- 1034 Feng, Z., 1997. Lithofacies palaeogeography of the Early and Middle Triassic of south China. *Chinese Journal of*
1035 *Geology*, 32(2): 212–220.
- 1036 Feng, Z., He, Y. and Wu, S., 1993. Lithofacies paleogeography of Permian of Middle and Lower Yangtze region.
1037 *Acta Sedimentologica Sinica*, 11(3): 13–24.
- 1038 Forel, M.-B., 2012. Ostracods (Crustacea) associated with microbialites across the Permian-Triassic boundary in
1039 Dajiang (Guizhou Province, south China). *European Journal of Taxonomy*(19): 1–34.
- 1040 Forel, M.-B., 2013. The Permian–Triassic mass extinction: ostracods (Crustacea) and microbialites. *Comptes*

- 1041 Rendus Geoscience, 345(4): 203–211.
- 1042 Forsey, G.F., 2013. Fossil evidence for the escalation and origin of marine mutualisms. *Journal of natural history*,
1043 47(25-28): 1833–1864.
- 1044 Foster, W., Lehrmann, D., Yu, M., Ji, L. and Martindale, R., 2018. Persistent environmental stress delayed the
1045 recovery of marine communities in the aftermath of the latest Permian mass extinction. *Paleoceanography*
1046 and *Paleoclimatology*, 33(4): 338–353.
- 1047 Foster, W.J., Lehrmann, D.J., Yu, M. and Martindale, R.C., 2019. Facies selectivity of benthic invertebrates in a
1048 Permian/Triassic boundary microbialite succession: Implications for the “microbialite refuge” hypothesis.
1049 *Geobiology*, 17(5): 523–535.
- 1050 Gaillot, J. and Vachard, D., 2007. The Khuff Formation (Middle East) and time-equivalents in Turkey and South
1051 China: biostratigraphy from Capitanian to Changhsingian times (Permian), new foraminiferal taxa, and
1052 palaeogeographical implications. *Coloquios de Paleontología*, 57(57): 37–223.
- 1053 Gaillot, J., Vachard, D., Galfetti, T. and Martini, R., 2009. New latest Permian foraminifers from Laren (Guangxi
1054 Province, South China): Palaeobiogeographic implications. *Geobios*, 42(2): 141–168.
- 1055 Gallagher, S.J., 1998. Controls on the distribution of calcareous Foraminifera in the Lower Carboniferous of
1056 Ireland. *Marine micropaleontology*, 34(3–4): 187–211.
- 1057 Gao, Y.Q., Yang, F.Q. and Peng, Y.Q., 2001. Late Permian deep water stratigraphy in Shaiwa of Ziyun, Guizhou.
1058 *Journal of Stratigraphy*, 25(2): 116–124.
- 1059 Glock, N., Roy, A.-S., Romero, D., Wein, T., Weissenbach, J., Revsbech, N.P., Høglund, S., Clemens, D., Sommer,
1060 S. and Dagan, T., 2019. Metabolic preference of nitrate over oxygen as an electron acceptor in
1061 foraminifera from the Peruvian oxygen minimum zone. *Proceedings of the National Academy of Sciences*,
1062 U.S.A., 116(8): 2860–2865.

- 1063 Glock, N., Schönfeld, J., Eisenhauer, A., Hensen, C., Mallon, J. and Sommer, S., 2013. The role of benthic
1064 foraminifera in the benthic nitrogen cycle of the Peruvian oxygen minimum zone. *Biogeosciences*, 10(7):
1065 4767–4783.
- 1066 Godbold, A., Schoepfer, S., Shen, S. and Henderson, C.M., 2017. Precarious ephemeral refugia during the earliest
1067 Triassic. *Geology*, 45(7): 607–610.
- 1068 Grasby, S.E., Sanei, H. and Beauchamp, B., 2011. Catastrophic dispersion of coal fly ash into oceans during the
1069 latest Permian extinction. *Nature Geoscience*, 4(2): 104–107.
- 1070 Grasby, S.E., Shen, W., Yin, R., Gleason, J.D., Blum, J.D., Lepak, R.F., Hurley, J.P. and Beauchamp, B., 2017.
1071 Isotopic signatures of mercury contamination in latest Permian oceans. *Geology*, 45(1): 55–58.
- 1072 Grice, K., Cao, C., Love, G.D., Böttcher, M.E., Twitchett, R.J., Grosjean, E., Summons, R.E., Turgeon, S.C.,
1073 Dunning, W. and Jin, Y., 2005. Photic zone euxinia during the Permian-Triassic superanoxic event.
1074 *Science*, 307(5710): 706–709.
- 1075 Groves, J.R. and Altiner, D., 2005. Survival and recovery of calcareous foraminifera pursuant to the end-Permian
1076 mass extinction. *Comptes Rendus Palevol*, 4(6): 487–500.
- 1077 Groves, J.R., Altiner, D. and Rettori, R., 2003. Origin and early evolutionary radiation of the Order Lagenida
1078 (Foraminifera). *Journal of Paleontology*, 77(5): 831–843.
- 1079 Groves, J.R., Altiner, D. and Rettori, R., 2005. Extinction, survival, and recovery of lagenide foraminifers in the
1080 Permian–Triassic boundary interval, Central Taurides, Turkey. *Journal of Paleontology*, 79(Jul 2005): 1-
1081 38.
- 1082 Groves, J.R., Payne, J.L. and Altiner, D., 2007. End-Permian Mass Extinction of Lagenide Foraminifers in the
1083 Southern Alps (Northern Italy). *Journal of Paleontology*, 81(3): 415-434.
- 1084 Groves, J.R. and Yue, W., 2009. Foraminiferal diversification during the late Paleozoic ice age. *Paleobiology*, 35(3):

- 1085 367–392.
- 1086 Gu, S., Feng, Q.L. and He, W., 2007. The Last Permian Deep-Water Fauna: Latest Changhsingian Small
1087 Foraminifers from Southwestern Guangxi, South China. *Micropaleontology*, 53(4): 311–330.
- 1088 Hammer, Ø., Harper, D. and Ryan, P., 2017. PAST: Paleontological Statistics. Version 3.16. National History
1089 Museum, University of Oslo, Oslo, 256 pp.
- 1090 Hammer, Ø. and Harper, D.A.T., 2006. *Paleontological Data Analysis*. Blackwell Publishing, Oxford.
- 1091 He, W., Feng, Q., Gu, S. and Jin, Y., 2005. Changxingian (Upper Permian) Radiolarian Fauna from Meishan D
1092 Section, Changxing, Zhejiang, China, and Its Possible Paleocological Significance. *Journal of*
1093 *Paleontology*, 79(2): 209–218.
- 1094 He, Y., Luo, J., Wen, Z., Liu, M. and Wang, Y., 2013. Lithofacies palaeogeography of the Upper Permian
1095 Changxing Stage in the Middle and Upper Yangtze Region, China. Elsevier.
- 1096 Hemleben, C., Kaminski, M.A., Kuhnt, W. and Scott, D.B., 1990. Paleocology, biostratigraphy,
1097 paleoceanography and taxonomy of agglutinated foraminifera, 327. Kluwer Academic Publishers, 1017
1098 pp.
- 1099 Hinojosa, J.L., Brown, S.T., Chen, J., Depaolo, D.J., Paytan, A., Shen, S. and Payne, J.L., 2012. Evidence for end-
1100 Permian ocean acidification from calcium isotopes in biogenic apatite. *Geology*, 40(8): 743–746.
- 1101 Hips, K. and Pelikán, P., 2002. Lower Triassic shallow marine succession in the Bükk Mountains, NE Hungary.
1102 *Geologica Carpathica*, 53(6): 351–367.
- 1103 Huang, Y., 2014. Extinction and Recovery of Bivalves during the Permian-Triassic Transition. Ph.D. Thesis, China
1104 university of Geosciences, Wuhan, 136 pp.
- 1105 Huang, Y., Tong, J. and Fraiser, M.L., 2018. A Griesbachian (Early Triassic) mollusc fauna from the Sidazhai
1106 section, Southwest China, with paleocological insights on the proliferation of genus *Claraia* (Bivalvia).

- 1107 Journal of Earth Science, 29(4): 794–805.
- 1108 Insalaco, E., Virgone, A., Courme, B., Gaillot, J., Kamali, M.R., Moallemi, A., Lotfpour, M. and Monibi, S., 2006.
- 1109 Upper Dalan Member and Kangan Formation between the Zagros Mountains and offshore Fars, Iran:
- 1110 Depositional system, biostratigraphy and stratigraphic architecture. *GeoArabia*, 11(2): 75–176.
- 1111 Isozaki, Y., 1997. Permo-Triassic boundary superanoxia and stratified superocean: records from lost deep sea.
- 1112 *Science*, 276(5310): 235–238.
- 1113 Ji, W., 2012. Lower-Middle Triassic Conodont biostratigraphy in slope-basin facies, South Guizhou. thesis Thesis,
- 1114 China University of Geosciences, Wuhan, 48 pp.
- 1115 Jia, E. and Song, H., 2018. End-Permian mass extinction of calcareous algae and microproblematica from
- 1116 Liangfengya, South China. *Geobios*, 51(5): 401–418.
- 1117 Jiang, H., Lai, X., Luo, G., Aldridge, R., Zhang, K. and Wignall, P., 2007. Restudy of conodont zonation and
- 1118 evolution across the P/T boundary at Meishan section, Changxing, Zhejiang, China. *Global and Planetary*
- 1119 *Change*, 55(1): 39–55.
- 1120 Jiang, H., Lai, X., Sun, Y., Wignall, P.B., Liu, J. and Yan, C., 2014. Permian-Triassic conodonts from Dajiang
- 1121 (Guizhou, South China) and their implication for the age of microbialite deposition in the aftermath of
- 1122 the End-Permian mass extinction. *Journal of Earth Science*, 25(3): 413–430.
- 1123 Jiang, H., Lai, X., Yan, C., Aldridge, R.J., Wignall, P. and Sun, Y., 2011. Revised conodont zonation and conodont
- 1124 evolution across the Permian–Triassic boundary at the Shangsi section, Guangyuan, Sichuan, South China.
- 1125 *Global and Planetary Change*, 77(3–4): 103–115.
- 1126 Jin, R., 1987. Radiolarites and sedimentary environments of the Late Permian Dalong Formation in the Northern
- 1127 sector of The Longmen Mountains, Sichuan Province. *Geological Review*, 33(3): 238–246.
- 1128 Jin, X. and Yang, X., 2004. Paleogeographic implications of the Shanita-Hemigordius fauna (Permian foraminifer)

- 1129 in the reconstruction of Permian Tethys. *Episodes*, 27(4): 273–278.
- 1130 Jin, Y., Wang, Y., Wang, W., Shang, Q., Cao, C. and Erwin, D., 2000. Pattern of marine mass extinction near the
1131 Permian-Triassic boundary in South China. *Science*, 289(5478): 432–436.
- 1132 Joachimski, M.M., Lai, X., Shen, S., Jiang, H., Luo, G., Chen, B., Chen, J. and Sun, Y., 2012. Climate warming in
1133 the latest Permian and the Permian-Triassic mass extinction. *Geology*, 40(3): 195–198.
- 1134 Kaiho, K., 1994. Benthic foraminiferal dissolved-oxygen index and dissolved-oxygen levels in the modern ocean.
1135 *Geology*, 22(8): 719–722.
- 1136 Kauffman, E.G. and Harries, P.J., 1996. The importance of crisis progenitors in recovery from mass extinction.
1137 Geological Society, London, Special Publications, 102(1): 15–39.
- 1138 Keller, G. and Kerr, A.C., 2014. *Volcanism, Impacts, and Mass Extinctions: Causes and Effects*, 505. Geological
1139 Society of America, 491 pp.
- 1140 Knoll, A.H., Bambach, R.K., Canfield, D.E. and Grotzinger, J.P., 1996. Comparative Earth History and Late
1141 Permian Mass Extinction. *Science*, 273(5274): 452.
- 1142 Knoll, A.H., Bambach, R.K., Payne, J.L., Pruss, S. and Fischer, W.W., 2007. Paleophysiology and end-Permian
1143 mass extinction. *Earth and Planetary Science Letters*, 256(3–4): 295–313.
- 1144 Kobayashi, F., 1997. Upper Permian foraminifers from the Iwai-Kanyo area, West Tokyo, Japan. *The Journal of*
1145 *Foraminiferal Research*, 27(3): 186–195.
- 1146 Kobayashi, F., 2006. Latest Permian (Changhsingian) foraminifers in the Mikata area, Hyogo—Late Paleozoic
1147 and Early Mesozoic foraminifers of Hyogo, Japan, Part 3. *Nature & Human Activities*, 10: 15–24.
- 1148 Kobayashi, F., 2012. Middle and Late Permian Foraminifers from the Chichibu Belt, Takachiho Area, Kyushu,
1149 Japan: Implications For Faunal Events PERMIAN FORAMINIFERS OF TAKACHIHO. *Journal of*
1150 *Paleontology*, 86(4): 669–687.

- 1151 Kobayashi, F., 2013. Late Permian (Lopingian) foraminifers from the Tsukumi Limestone, southern Chichibu
1152 Terrane of eastern Kyushu, Japan. *The Journal of Foraminiferal Research*, 43(2): 154-169.
- 1153 Kobayashi, F. and Ishii, K.-I., 2003. Paleobiogeographic analysis of Yahtashian to Midian fusulinacean faunas of
1154 the Surmaq Formation in the Abadeh region, central Iran. *The Journal of Foraminiferal Research*, 33(2):
1155 155–165.
- 1156 Kolar-Jurkovšek, T., Vuks, V.J., Aljinović, D., Hautmann, M., Kaim, A. and Jurkovšek, B., 2013. Olenekian (Early
1157 Triassic) fossil assemblage from eastern Julian Alps (Slovenia), *Annales Societatis Geologorum Poloniae*,
1158 pp. 213–227.
- 1159 Kolodka, C., Vennin, E., Vachard, D., Trocme, V. and Goodarzi, M.H., 2012. Timing and progression of the end-
1160 Guadalupian crisis in the Fars province (Dalan Formation, Kuh-e Gakhum, Iran) constrained by
1161 foraminifers and other carbonate microfossils. *Facies*, 58(1): 131–153.
- 1162 Lai, X., Yang, F.Q., Hallam, A. and Wignall, P.B., 1996. The Shangsi section, candidate of the global stratotype
1163 section and point of the Permian–Triassic boundary. In: H. Yin (Editor), *The Palaeozoic–Mesozoic*
1164 *boundary, candidates of the global stratotype section and point of the Permian–Triassic boundary*. China
1165 University of Geosciences Press, Wuhan, pp. 113–124.
- 1166 Lee, J. and Hallock, P., 1987. Algal Symbiosis as the Driving Force in the Evolution of Larger Foraminifera a.
1167 *Annals of the New York Academy of Sciences*, 503(Endocytobiology): 330–347.
- 1168 Lee, J., McEnergy, M., Kahn, E. and Schuster, F., 1979. Symbiosis and the evolution of larger foraminifera.
1169 *Micropaleontology*, 25(2): 118–140.
- 1170 Lee, J.J., Cervasco, M.H., Morales, J., Billik, M., Fine, M. and Levy, O., 2010. Symbiosis drove cellular evolution.
1171 *Symbiosis*, 51(1): 13–25.
- 1172 Lehrmann, D.J., 1999. Early Triassic calcimicrobial mounds and biostromes of the Nanpanjiang basin, south China.

1173 Geology, 27(4): 359–362.

1174 Lehrmann, D.J., Bentz, J.M., Wood, T., Goers, A., Dhillon, R., Akin, S., Xiaowei, L.I., Payne, J.L., Kelley, B.M.
1175 and Meyer, K.M., 2015. Environmental controls on the genesis of marine microbialites and dissolution
1176 surface associated with the end-Permian mass extinction: new sections and observations from the
1177 Nanpanjiang Basin, South China. *Palaios*, 30(7): 529–552.

1178 Lehrmann, D.J., Payne, J.L., Felix, S.V., Dillett, P.M., Wang, H., Yu, Y. and Wei, J., 2003. Permian–Triassic
1179 boundary sections from shallow-marine carbonate platforms of the Nanpanjiang Basin, South China:
1180 implications for oceanic conditions associated with the end-Permian extinction and its aftermath. *Palaios*,
1181 18(2): 138–152.

1182 Lehrmann, D.J., Wei, J. and Enos, P., 1998. Controls on facies architecture of a large Triassic carbonate platform;
1183 the Great Bank of Guizhou, Nanpanjiang Basin, South China. *Journal of Sedimentary Research*, 68(2):
1184 311–326.

1185 Li, Z., Zhan, L., Zhu, X., Zhang, J., Jin, R., Liu, G., Shen, H., Shen, G., Dai, J., Huang, H., Xie, L. and Yan, Z.,
1186 1986. Mass extinction and geological events between Paleozoic and Mesozoic era. *Acta Geological*
1187 *Sinica*(1): 1–15.

1188 Lin, J., Li, J. and Sun, Q., 1990. Late Paleozoic Foraminifera in South China. Science Press, Beijing, 297 pp.

1189 Liu, J.B., Ezaki, Y., Yang, S.R., Wang, H.F. and Adachi, N., 2007. Age and sedimentology of microbialites after
1190 the end-Permian mass extinction in Luodian, Guizhou Province. *Journal of Palaeogeography*, 9(5): 473–
1191 486.

1192 Loeblich, A.R. and Tappan, H., 1988. Foraminiferal genera and their classification. Van Nostrand Reinhold
1193 Company, New York, 970 pp.

1194 Loeblich, A.R. and Tappan, H., 1992. Present status of foraminiferal classification. In: Y. Takayanagi and T. Saito

- 1195 (Editors), *Studies in Benthic Foraminifera, Benthos' 90*, Sendai, 1990. Tokai University Press, Tokyo, pp.
- 1196 93-102.
- 1197 Luo, G., Wang, Y., Algeo, T.J., Kump, L.R., Bai, X., Yang, H., Yao, L. and Xie, S., 2011. Enhanced nitrogen
- 1198 fixation in the immediate aftermath of the latest Permian marine mass extinction. *Geology*, 39(7): 647–
- 1199 650.
- 1200 Luo, G., Wang, Y., Grice, K., Kershaw, S., Algeo, T.J., Ruan, X., Yang, H., Jia, C. and Xie, S., 2013. Microbial–
- 1201 algal community changes during the latest Permian ecological crisis: Evidence from lipid biomarkers at
- 1202 Cili, South China. *Global and Planetary Change*, 105(Supplement C): 36–51.
- 1203 MacLeod, K.G., Quinton, P.C. and Bassett, D.J., 2017. Warming and increased aridity during the earliest Triassic
- 1204 in the Karoo Basin, South Africa. *Geology*, 45(6): 483–486.
- 1205 Marshall, C.R., 1990. Confidence intervals on stratigraphic ranges. *Paleobiology*, 16(1): 1–10.
- 1206 Marshall, C.R. and Ward, P.D., 1996. Sudden and gradual molluscan extinctions in the latest Cretaceous of western
- 1207 European Tethys. *Science*, 274(5291): 1360–1363.
- 1208 McGhee, G.R., Clapham, M.E., Sheehan, P.M., Bottjer, D.J. and Droser, M.L., 2013. A new ecological-severity
- 1209 ranking of major Phanerozoic biodiversity crises. *Palaeogeography, Palaeoclimatology, Palaeoecology*,
- 1210 370: 260–270.
- 1211 McKinney, M.L., 1997. Extinction vulnerability and selectivity: combining ecological and paleontological views.
- 1212 *Annual Review of Ecology and Systematics*, 28(1): 495–516.
- 1213 Meldahl, K.H., 1990. Sampling, species abundance, and the stratigraphic signature, of mass extinction: A test using
- 1214 Holocene tidal flat molluscs. *Geology*, 18(9): 890–893.
- 1215 Meyer, K., Yu, M., Jost, A., Kelley, B. and Payne, J., 2011. $\delta^{13}\text{C}$ evidence that high primary productivity delayed
- 1216 recovery from end-Permian mass extinction. *Earth and Planetary Science Letters*, 302(3–4): 378–384.

- 1217 Miao, L., Dai, X., Korn, D., Brayard, A., Chen, J., Liu, X. and Song, H., 2019. A Changhsingian (late Permian)
1218 nautiloid assemblage from Gujiao, South China. *Papers in Palaeontology*, n/a(n/a).
- 1219 Mohtat-Aghaï, P. and Vachard, D., 2005. Late Permian foraminiferal assemblages from the Hambast region
1220 (central Iran) and their extinctions. *Revista Española De Micropaleontología*, 37(2): 205–227.
- 1221 Murray, J.W., 2006. *Ecology and applications of benthic foraminifera*. Cambridge University Press, New York,
1222 426 pp.
- 1223 Nejad, M.E., Vachard, D., Siabeghodsy, A.A. and Abbasi, S., 2015. Middle-Late Permian (Murgabian-Djulfian)
1224 foraminifers of the northern Maku area (western Azerbaijan, Iran). *Palaeontologia Electronica*, 18(1): 1–
1225 63.
- 1226 Nestell, G.P., Kolar-Jurkovšek, T., Jurkovšek, B. and Aljinović, D., 2011. Foraminifera from the Permian-Triassic
1227 transition in western Slovenia. *Micropaleontology*, 57(3): 197–222.
- 1228 Nigam, R., Kurtarkar, S., R, Linshy, V. and Rana, S., 2008. Response of benthic foraminifera *Rosalina leei* to
1229 different temperature and salinity, under laboratory culture experiment. *Journal of the Marine Biological*
1230 *Association of the UK*, 88(4): 699–704.
- 1231 Novacek, M., 2001. *The biodiversity crisis: losing what counts*. New Press, 223 pp.
- 1232 Osleger, D. and Read, J.F., 1991. Relation of eustasy to stacking patterns of meter-scale carbonate cycles, Late
1233 Cambrian, USA. *Journal of Sedimentary Research*, 61(7): 1225–1252.
- 1234 Pörtner, H.-O., 2010. Oxygen-and capacity-limitation of thermal tolerance: a matrix for integrating climate-related
1235 stressor effects in marine ecosystems. *Journal of Experimental Biology*, 213(6): 881–893.
- 1236 Pörtner, H.O. and Knust, R., 2007. Climate change affects marine fishes through the oxygen limitation of thermal
1237 tolerance. *Science*, 315(5808): 95–97.
- 1238 Parker, W.C. and Arnold, A.J., 2003. Quantitative methods of data analysis in foraminiferal ecology, *Modern*

- 1239 Foraminifera. Springer Netherlands, Dordrecht, pp. 71–89.
- 1240 Payne, J.L., Lehrmann, D.J., Wei, J., Orchard, M.J., Schrag, D.P. and Knoll, A.H., 2004. Large perturbations of
1241 the carbon cycle during recovery from the end-Permian extinction. *Science*, 305(5683): 506–509.
- 1242 Payne, J.L., Summers, M., Rego, B.L., Altiner, D., Wei, J., Yu, M. and Lehrmann, D.J., 2011. Early and Middle
1243 Triassic trends in diversity, evenness, and size of foraminifers on a carbonate platform in south China:
1244 implications for tempo and mode of biotic recovery from the end-Permian mass extinction. *Paleobiology*,
1245 37(3): 409–425.
- 1246 Payne, J.L., Turchyn, A.V., Paytan, A., Depaolo, D.J., Lehrmann, D.J., Yu, M. and Wei, J., 2010. Calcium isotope
1247 constraints on the end-Permian mass extinction. *Proceedings of the National Academy of Sciences of the*
1248 *United States of America*, 107(19): 8543–8548.
- 1249 Peng, Y.Q. and Tong, J.N., 1999. Integrated Study on Permian-Triassic Boundary Bed in Yangtze Platform. *Earth*
1250 *Science*, 24(1): 39–48.
- 1251 Penn, J.L., Deutsch, C., Payne, J.L. and Sperling, E.A., 2018. Temperature-dependent hypoxia explains
1252 biogeography and severity of end-Permian marine mass extinction. *Science*, 362(6419): eaat1327.
- 1253 Piña-Ochoa, E., Høglund, S., Geslin, E., Cedhagen, T., Revsbech, N.P., Nielsen, L.P., Schweizer, M., Jorissen, F.,
1254 Rysgaard, S. and Risgaard-Petersen, N., 2010. Widespread occurrence of nitrate storage and
1255 denitrification among Foraminifera and Gromiida. *Proceedings of the National Academy of Sciences*,
1256 *U.S.A.*, 107(3): 1148–1153.
- 1257 Pronina-Nestell, G.P. and Nestell, M.K., 2001. Late Changhsingian Foraminifers of the Northwestern Caucasus.
1258 *Micropaleontology*, 47(3): 205–234.
- 1259 Pronina, G., 1988. The Late Permian foraminifers of Transcaucasus. *Revue de paleobiologie*, 2: 89–96.
- 1260 Rampino, M.R. and Adler, A.C., 1998. Evidence for abrupt latest Permian mass extinction of foraminifera: results

- 1261 of tests for the Signor-Lipps effect. *Geology*, 26(5): 415–418.
- 1262 Raup, D.M., 1975. Taxonomic diversity estimation using rarefaction. *Paleobiology*, 1(4): 333–342.
- 1263 Renne, P.R. and Basu, A.R., 1995. Synchrony and causal relations between permian-triassic boundary crises and
1264 siberian flood volcanism. *Science*, 269(5229): 1413–1416.
- 1265 Risgaard-Petersen, N., Langezaal, A.M., Ingvarnsen, S., Schmid, M.C., Jetten, M.S., den Camp, H.J.O., Derksen,
1266 J.W., Pina-Ochoa, E., Eriksson, S.P. and Nielsen, L.P., 2006. Evidence for complete denitrification in a
1267 benthic foraminifer. *Nature*, 443(7107): 93–96.
- 1268 Robertson, D.S., McKenna, M.C., Toon, O.B., Hope, S. and Lillegraven, J.A., 2004. Survival in the first hours of
1269 the Cenozoic. *Geological Society of America Bulletin*, 116(5–6): 760–768.
- 1270 Sakagami, S. and Hatta, A., 1982. On the Upper Permian Palaeofusulina-Colaniella fauna from Khao Doi Pha
1271 Phlung, North Thailand, *Geology and Palaeontology of Southeast Asia*. University of Tokyo Press, pp.
1272 1–14.
- 1273 Sanei, H., Grasby, S.E. and Beauchamp, B., 2012. Latest Permian mercury anomalies. *Geology*, 40(1): 63–66.
- 1274 Saraswat, R., Nigam, R. and Pachkhande, S., 2011. Difference in optimum temperature for growth and
1275 reproduction in benthic foraminifer *Rosalina globularis*: Implications for paleoclimatic studies. *Journal*
1276 *of Experimental Marine Biology and Ecology*, 405(1): 105–110.
- 1277 Schröder-Adams, C.J., Boyd, R., Ruming, K. and Sandstrom, M., 2008. Influence of sediment transport dynamics
1278 and ocean floor morphology on benthic foraminifera, offshore Fraser Island, Australia. *Marine Geology*,
1279 254(1): 47–61.
- 1280 Scotese, C.R., 2001. Atlas of earth history. University of Texas at Arlington. Department of Geology. PALEOMAP
1281 Project, Texas, 58 pp.
- 1282 Sepkoski, J.J., 1981. A factor analytic description of the Phanerozoic marine fossil record. *Paleobiology*, 7(1): 36–

- 1283 53.
- 1284 Setoyama, E., Kaminski, M.A. and Tyszka, J., 2011. The Late Cretaceous–Early Paleocene palaeobathymetric
1285 trends in the southwestern Barents Sea — Palaeoenvironmental implications of benthic foraminiferal
1286 assemblage analysis. *Palaeogeography, Palaeoclimatology, Palaeoecology*, 307(1): 44–58.
- 1287 Shen, J., Chen, J., Algeo, T.J., Yuan, S., Feng, Q., Yu, J., Zhou, L., O’Connell, B. and Planavsky, N.J., 2019.
1288 Evidence for a prolonged Permian–Triassic extinction interval from global marine mercury records.
1289 *Nature Communications*, 10(1): 1563.
- 1290 Shen, J., Feng, Q., Algeo, T.J., Li, C., Planavsky, N.J., Zhou, L. and Zhang, M., 2016. Two pulses of oceanic
1291 environmental disturbance during the Permian–Triassic boundary crisis. *Earth & Planetary Science*
1292 *Letters*, 443: 139–152.
- 1293 Shen, S., Ramezani, J., Chen, J., Cao, C., Erwin, D., Zhang, H., Xiang, L., Schoepfer, S., Henderson, C. and Zheng,
1294 Q., 2018. A sudden end-Permian mass extinction in South China. *Geological Society of America Bulletin*,
1295 131(1–2): 205–223.
- 1296 Shen, Y., Farquhar, J., Zhang, H., Masterson, A., Zhang, T. and Wing, B.A., 2011. Multiple S-isotopic evidence
1297 for episodic shoaling of anoxic water during Late Permian mass extinction. *Nature Communications*, 2(1):
1298 1–5.
- 1299 Sheng, J., Chen, C., Wang, Y., Rui, L., Liao, Z., Bando, Y., Ishii, K., Nakazawa, K. and Nakamura, K., 1984.
1300 Permian-Triassic boundary in middle and eastern Tethys. *Journal of the Faculty of Science, Hokkaido*
1301 *University*, 4(21): 133–81.
- 1302 Song, H., Tong, J. and Chen, Z., 2009a. Two episodes of foraminiferal extinction near the Permian–Triassic
1303 boundary at the Meishan section, South China. *Australian Journal of Earth Sciences*, 56(6): 765–773.
- 1304 Song, H., Tong, J., Chen, Z., Yang, H. and Wang, Y., 2009b. End-Permian mass extinction of foraminifers in the

- 1305 Nanpanjiang Basin, South China. *Journal of Paleontology*, 83(5): 718–738.
- 1306 Song, H., Tong, J. and Chen, Z.Q., 2011a. Evolutionary dynamics of the Permian–Triassic foraminifer size:
1307 Evidence for Lilliput effect in the end-Permian mass extinction and its aftermath. *Palaeogeography*
1308 *Palaeoclimatology Palaeoecology*, 308(1–2): 98–110.
- 1309 Song, H., Tong, J., Wignall, P.B., Luo, M.A.O., Tian, L.I., Song, H., Huang, Y. and Chu, D., 2016. Early Triassic
1310 disaster and opportunistic foraminifers in South China. *Geological Magazine*, 153(2): 298–315.
- 1311 Song, H., Tong, J., Zhang, K., Wang, Q. and Chen, Z.Q., 2007. Foraminiferal survivors from the Permian-Triassic
1312 mass extinction in the Meishan section, South China. *Palaeoworld*, 16(1): 105-119.
- 1313 Song, H., Wignall, P.B., Chen, Z.-Q., Tong, J., Bond, D.P., Lai, X., Zhao, X., Jiang, H., Yan, C. and Niu, Z., 2011b.
1314 Recovery tempo and pattern of marine ecosystems after the end-Permian mass extinction. *Geology*, 39(8):
1315 739–742.
- 1316 Song, H., Wignall, P.B., Chu, D., Tong, J., Sun, Y., Song, H., He, W. and Tian, L., 2014. Anoxia/high temperature
1317 double whammy during the Permian-Triassic marine crisis and its aftermath. *Scientific Reports*, 4(2):
1318 4132.
- 1319 Song, H., Wignall, P.B. and Dunhill, A.M., 2018. Decoupled taxonomic and ecological recoveries from the Permo-
1320 Triassic extinction. *Science Advances*, 4(10): eaat5091.
- 1321 Song, H., Wignall, P.B., Tong, J., Bond, D.P., Song, H., Lai, X., Zhang, K., Wang, H. and Chen, Y., 2012.
1322 Geochemical evidence from bio-apatite for multiple oceanic anoxic events during Permian–Triassic
1323 transition and the link with end-Permian extinction and recovery. *Earth and Planetary Science Letters*,
1324 353: 12–21.
- 1325 Song, H., Wignall, P.B., Tong, J. and Yin, H., 2013. Two pulses of extinction during the Permian-Triassic crisis.
1326 *Nature Geoscience*, 6(1): 52–56.

- 1327 Song, H., Yang, L., Tong, J., Chen, J., Tian, L., Song, H. and Chu, D., 2015. Recovery dynamics of foraminifers
1328 and algae following the Permian-Triassic extinction in Qingyan, South China. *Geobios*, 48(1): 71–83.
- 1329 Stanley, S. and Yang, X., 1994. A double mass extinction at the end of the Paleozoic Era. *Science*, 266(5189):
1330 1340–1344.
- 1331 Strauss, D. and Sadler, P.M., 1989. Classical confidence intervals and Bayesian probability estimates for ends of
1332 local taxon ranges. *Mathematical Geology*, 21(4): 411–427.
- 1333 Sun, Y., Joachimski, M.M., Wignall, P.B., Yan, C., Chen, Y., Jiang, H., Wang, L. and Lai, X., 2012. Lethally hot
1334 temperatures during the Early Triassic greenhouse. *Science*, 338(6105): 366–370.
- 1335 Sun, Y., Zulla, M., Joachimski, M., Bond, D., Wignall, P., Zhang, Z. and Zhang, M., 2019. Ammonium ocean
1336 following the end-Permian mass extinction. *Earth and Planetary Science Letters*, 518: 211–222.
- 1337 Tappan, H. and Loeblich, A.R., 1988. Foraminiferal Evolution, Diversification, and Extinction. *Journal of*
1338 *Paleontology*, 62(5): 695–714.
- 1339 Teichert, C., Kummel, B. and Kapoor, H., 1970. Mixed Permian-Triassic fauna, Guryul Ravine, Kashmir. *Science*,
1340 167(3915): 174–175.
- 1341 Tong, J. and Kuang, W., 1990. A study of the Changxingian foraminifera and microfacies in Liangfengya,
1342 Chongqing, Sichuan Province. *Earth Science-Journal of China University of Geosciences*, 15(3): 337–
1343 344.
- 1344 Tong, J. and Shi, G., 2000. Evolution of the Permian and Triassic foraminifera in South China. In: H. Yin, J.M.
1345 Dickins, G.R. Shi and J. Tong (Editors), *Permian–Triassic evolution of Tethys and Western Circum*
1346 *Pacific*. Elsevier, pp. 291–307.
- 1347 Vachard, D., 2016. Permian smaller foraminifers: taxonomy, biostratigraphy and biogeography. *Geological Society*
1348 *London Special Publications*, 450(1): 205–252.

- 1349 Vachard, D. and Miconnet, P., 1989. Une association a fusulinoides du Murghabien superieur au Monte Facito
1350 (Apennin meridional, Italie). *Revue de Micropaleontologie*, 32(4): 297–318.
- 1351 Vachard, D. and Moix, P., 2013. Kubergandian (Roadian, Middle Permian) of the Lycian and Aladağ Nappes
1352 (Southern Turkey). *Geobios*, 46(4): 335–356.
- 1353 Vachard, D., Pille, L. and Gaillot, J., 2010. Palaeozoic Foraminifera: Systematics, palaeoecology and responses to
1354 global changes. *Revue De Micropaléontologie*, 53(4): 209–254.
- 1355 Vuks, V.J., 2000. Triassic foraminifers of the Crimea, Caucasus, Mangyshlak and Pamirs (biostratigraphy and
1356 correlation). *Zentralblatt für Geologie und Paläontologie Teil I*, 11-12: 1353–1365.
- 1357 Vuks, V.J., 2007. Olenekian (Early Triassic) foraminifers of the Gorny Mangyshlak, eastern Precaucasus and
1358 western Caucasus. *Palaeogeography, Palaeoclimatology, Palaeoecology*, 252(1–2): 82–92.
- 1359 Waldrop, M.M., 1988. After the fall: although the dust was bad, the chemical fallout from the Cretaceous-Tertiary
1360 impact was worse-much worse. *Science*, 239(4843): 977–978.
- 1361 Wan, J., Yuan, A., Crasquin, S., Jiang, H., Yang, H. and Hu, X., 2019. High-resolution variation in ostracod
1362 assemblages from microbialites near the Permian-Triassic boundary at Zuodeng, Guangxi region, South
1363 China. *Palaeogeography, Palaeoclimatology, Palaeoecology*, 535: 109349.
- 1364 Wang, L., Wignall, P.B., Wang, Y., Jiang, H., Sun, Y., Li, G., Yuan, J. and Lai, X., 2016. Depositional conditions
1365 and revised age of the Permo-Triassic microbialites at Gaohua section, Cili County (Hunan Province,
1366 South China). *Palaeogeography, Palaeoclimatology, Palaeoecology*, 443: 156–166.
- 1367 Wang, Q., Tong, J., Song, H. and Yang, H., 2009. Ecological evolution across the Permian/Triassic boundary at
1368 the Kangjiaping Section in Cili County, Hunan Province, China. *Science in China Series D: Earth
1369 Sciences*, 52(6): 797–806.
- 1370 Wang, S.C. and Everson, P.J., 2007. Confidence intervals for pulsed mass extinction events. *Paleobiology*, 33(2):

- 1371 324–336.
- 1372 Wang, S.C. and Marshall, C.R., 2004. Improved confidence intervals for estimating the position of a mass
1373 extinction boundary. *Paleobiology*, 30(1): 5–18.
- 1374 Wang, Y. and Ueno, K., 2009. A new fusulinoidean genus *Dilatofusulina* from the Lopingian (Upper Permian) of
1375 southern Tibet, China. *The Journal of Foraminiferal Research*, 39(1): 56–65.
- 1376 Wang, Y., Ueno, K., Zhang, Y.c. and Cao, C.q., 2010. The Changhsingian foraminiferal fauna of a Neotethyan
1377 seamount: the Gyanyima Limestone along the Yarlung - Zangbo Suture in southern Tibet, China.
1378 *Geological Journal*, 45(2 - 3): 308 - 318.
- 1379 Wang, Y., Xu, G. and Lin, Q., 1997. Paleocological relations between coral reef and sponge reef of Late Permian
1380 in Cili area, West Hunan Province. *Earth Science*, 22(2): 135–138.
- 1381 Wignall, P., Hallam, A., Xulong, L. and Fengqing, Y., 1995. Palaeoenvironmental changes across the
1382 Permian/Triassic boundary at Shangsi (N. Sichuan, China). *Historical Biology*, 10(2): 175–189.
- 1383 Wignall, P.B. and Hallam, A., 1996. Facies change and the end-Permian mass extinction in SE Sichuan, China.
1384 *Palaios*, 11: 587–596.
- 1385 Wignall, P.B. and Twitchett, R.J., 1996. Oceanic anoxia and the end Permian mass extinction. *Science*, 272(5265):
1386 1155–1158.
- 1387 Winguth, A.M., Shields, C.A. and Winguth, C., 2015. Transition into a Hothouse World at the Permian-Triassic
1388 boundary-A model study. *Palaeogeography, Palaeoclimatology, Palaeoecology*, 440: 316–327.
- 1389 Woehle, C., Roy, A.-S., Glock, N., Wein, T., Weissenbach, J., Rosenstiel, P., Hiebenthal, C., Michels, J., Schönfeld,
1390 J. and Dagan, T., 2018. A novel eukaryotic denitrification pathway in foraminifera. *Current Biology*,
1391 28(16): 2536–2543. e5.
- 1392 Wu, H., Zhang, S., Hinnov, L.A., Jiang, G., Feng, Q., Li, H. and Yang, T., 2013. Time-calibrated Milankovitch

- 1393 cycles for the late Permian. *Nature Communications*, 4: 2452.
- 1394 Wu, S., 1988. Characteristics of stratigraphical and faunal changes near the Permo-Triassic boundary in the
1395 Huayingshan area, Sichuan Province. *Geoscience*, 2(3): 375–385.
- 1396 Xie, S., Algeo, T.J., Zhou, W., Ruan, X., Luo, G., Huang, J. and Yan, J., 2017. Contrasting microbial community
1397 changes during mass extinctions at the Middle/Late Permian and Permian/Triassic boundaries. *Earth and
1398 Planetary Science Letters*, 460: 180–191.
- 1399 Yang, H., Chen, Z., Wang, Y., Tong, J., Song, H. and Chen, J., 2011. Composition and structure of microbialite
1400 ecosystems following the end-Permian mass extinction in South China. *Palaeogeography,
1401 Palaeoclimatology, Palaeoecology*, 308(1–2): 111–128.
- 1402 Yang, L., Song, H., Tong, J., Chu, D., Liang, L., Kui, W.U. and Tian, L., 2016. The extinction pattern of
1403 foraminifers during the Permian-Triassic crisis at the Maochang section, Ziyun, Guizhou province, South
1404 China. *Acta Micropalaeontologica Sinica*, 33(3): 229–251.
- 1405 Yang, L., Song, H., Tong, J., Chu, D. and Tian, L., 2013. The extinction pattern of fusulinids during the Permian-
1406 Triassic crisis at the Ksangjiaping section, Cili, Hunan province. *Acta Micropalaeontologica Sinica*, 30(4):
1407 353–366.
- 1408 Yang, X., Jiarun, L. and Guijun, S., 2004. Extinction process and patterns of Middle Permian fusulinaceans in
1409 southwest China. *Lethaia*, 37(2): 139–147.
- 1410 Yang, Z., Yin, H., Wu, S., Yang, F., Ding, M. and Xu, G., 1987. Permian-Triassic boundary stratigraphy and fauna
1411 of South China. Geological Publishing House, Beijing, 379 pp.
- 1412 Yin, H., Jiang, H., Xia, W., Feng, Q., Zhang, N. and Shen, J., 2014. The end-Permian regression in South China
1413 and its implication on mass extinction. *Earth-Science Reviews*, 137: 19–33.
- 1414 Yin, H. and Song, H., 2013. Mass extinction and Pangea integration during the Paleozoic-Mesozoic transition.

- 1415 Science China Earth Sciences, 56(11): 1791–1803.
- 1416 Yin, H. and Wu, S., 1985. Transitional Bed—the basal Triassic unit of South China. Journal of China University
1417 of Geosciences, 10: 163–172.
- 1418 Yin, H., Zhang, K., Tong, J., Yang, Z. and Wu, S., 2001. The global stratotype section and point (GSSP) of the
1419 Permian-Triassic boundary. Episodes, 24(2): 102–114.
- 1420 Yuan, D.-x., Chen, J., Zhang, Y.-c., Zheng, Q.-f. and Shen, S.-z., 2015. Changhsingian conodont succession and
1421 the end-Permian mass extinction event at the Daijiagou section in Chongqing, Southwest China. Journal
1422 of Asian Earth Sciences, 105: 234–251.
- 1423 Yuan, D.-X., Shen, S.-z., Henderson, C.M., Chen, J., Zhang, H., Zheng, Q.-f. and Wu, H., 2019. Integrative
1424 timescale for the Lopingian (Late Permian): A review and update from Shangsi, South China. Earth-
1425 Science Reviews, 188: 190–209.
- 1426 Yuan, D.X. and Shen, S.Z., 2011. Conodont succession across the Permian-Triassic boundary of the Liangfengya
1427 section, Chongqing, south China. Acta Palaeontologica Sinica, 50(4): 420–438.
- 1428 Zhang, K., Tong, J., Yin, H. and Wu, S., 1996. Sequence stratigraphy of the Permian-Triassic boundary section of
1429 Changxing, Zhejiang. Acta Geologica Sinica, 70(3): 270–281.
- 1430 Zhang, M., 2015. Late Permian deep water foraminifal fauna from South China. Ph.D. Thesis, China University
1431 of Geosciences, Wuhan, 171 pp.
- 1432 Zhang, M. and Gu, S., 2015. Latest Permian deep-water foraminifers from Daxiakou, Hubei, South China. Journal
1433 of Paleontology, 89(3): 448–464.
- 1434 Zhang, Y.-c., Shen, S.-z., Zhang, Y.-j., Zhu, T.-x. and An, X.-y., 2016. Middle Permian non-fusuline foraminifers
1435 from the middle part of the Xiala Formation in Xainza county, Lhasa Block, Tibet. The Journal of
1436 Foraminiferal Research, 46(2): 99–114.

- 1437 Zhang, Y.-C., Wang, Y., Zhang, Y.-J. and Yuan, D.-X., 2013. Artinskian (Early Permian) fusuline fauna from the
1438 Rongma area in northern Tibet: palaeoclimatic and palaeobiogeographic implications. *Alcheringa: An*
1439 *Australasian Journal of Palaeontology*, 37(4): 529–546.
- 1440 Zhang, Y.C. and Yue, W., 2017. Permian fusuline biostratigraphy. In: G.S. Lucas and S.Z. Shen (Editors), *The*
1441 *Permian Timescale*. Geological Society, London, pp. 253–288.
- 1442 Zheng, Z., 1981. Uppermost Permian (Changhsingian) ammonoids from Western Guizhou. *Acta Palaeontologica*
1443 *Sinica*, 20(2): 107–113.
- 1444

1445 **The list of figure/table captions:**

1446 **Fig. 1.** Palaeogeographic map for the Permian-Triassic boundary interval. (A) Locations of studied sections
1447 in South China, modified from [Feng, \(1997\)](#), [Lehrmann et al. \(1998\)](#) and [He et al. \(2013\)](#). (B) Global map
1448 modified from [Scotese \(2001\)](#). (C) Schematic cross-section of the South China Block in the Permian-Triassic
1449 boundary interval showing the relative water depths of our seven study sections. Red stars show the locations
1450 of study sections. Abbreviations: NBYP = Northern Basin of the Yangtze Platform; NPJB = Nanpanjiang
1451 Basin; GBG = Great Bank of Guizhou.

1452 **Fig. 2.** Columnar sections of the Permian–Triassic successions at Cili, Dajiang, Liangfengya, Meishan,
1453 Shangsi, Gujiao, and Sidazhai. Biostratigraphic data of the Dajiang section from [Jiang et al. \(2014\)](#) and [Payne
1454 et al. \(2004\)](#), the Cili section from [Wang et al. \(2016\)](#), the Liangfengya section from [Yuan and Shen \(2011\)](#)
1455 and [Wu \(1988\)](#), the Meishan section from [Yin et al. \(2001\)](#), and [Jiang et al. \(2007\)](#), the Shangsi section from
1456 [Jiang et al. \(2011\)](#), [Yuan et al. \(2019\)](#), and [Lai et al. \(1996\)](#), the Gujiao section from [Dai et al. \(2018a\)](#) and
1457 unpublished data, and the Sidazhai section from [Huang \(2014\)](#) and [Ji \(2012\)](#) are followed herein. The blue
1458 box represents the late Changhsingian; the grey box represents the PTB interval; the pink box represents the
1459 late Griesbachian. Abbreviations: *C. yini* = *Clarkina yini*; *C. mei.* = *C. meishanensis*; *H. cha.* = *Hindeodus
1460 changxingensis*; *C. tay.* = *C. taylorae*; *H. par.* = *H. parvus*. *I. isarcica* = *Isarcicella isarcicai*.

1461 **Fig. 3.** Stratigraphic occurrences of foraminifers in the Cili section. The red lines represent 50% confidence
1462 intervals of each species. Contours indicating the predicted position of the extinction horizon are shown in
1463 grey bars. The horizontal black lines to the right of the lithologic column represent the sampling position. A
1464 list of foraminifers identified from Cili is provided as a Supplementary Table.

1465 **Fig. 4.** Stratigraphic occurrences of foraminifers at the Liangfengya section. The red lines represent 50%
1466 confidence intervals of each species. Contours indicating predicted positions of the extinction horizon are
1467 shown in grey bars. A list of foraminifers identified from Liangfengya is provided as a Supplementary Table.

1468 **Fig. 5.** Stratigraphic occurrences of foraminifers in the Shangsi section. A list of foraminifers identified at
1469 Shangsi is provided in a Supplementary Table.

1470 **Fig. 6.** Stratigraphic occurrences of foraminifers in the Gujiao section. A list of foraminifers identified at
1471 Gujiao is provided in a Supplementary Table.

1472 **Fig. 7.** Stratigraphic occurrences of foraminifers in the Sidazhai section. A list of foraminifers identified from
1473 Sidazhai is provided in a Supplementary Table.

1474 **Fig. 8.** Dendograms of Q-model cluster analyses of the seven sections, tested during the *C. yini* Zone (A),
1475 the PTB interval (B), and the late Griesbachian (C). Blue fonts represent platform foraminiferal assemblages.
1476 Orange-red fonts represent slope foraminiferal assemblages. Pink fonts represent basin foraminiferal
1477 assemblages. Abbreviations: DJ = Dajiang; CL = Cili; LFY = Liangfengya; MS = Meishan; SS = Shangsi;
1478 GJ = Gujiao; SDZ = Sidazhai.

1479 **Fig. 9.** A schematic diagram illustrating the percentage distribution of the dominant genera with depth in the
1480 late Changhsingian of South China. Abbreviations as in Fig. 8 caption. Indigo-blue boxes represent the Order
1481 Fusulinida. Orange boxes represent the Order Lagenida. Sky-blue boxes represent the Order Miliolida. Purple
1482 boxes represent the Order Textulariida.

1483 **Fig. 10.** The percentage distribution of dominant foraminifer genera with depth in the PTB interval in South

1484 China. Abbreviations as in Fig. 8 caption. Colours follow Fig. 9.

1485 **Fig. 11.** The percentage distribution of dominant foraminifer genera with depth in the late Griesbachian of
1486 South China. Abbreviations as in Fig. 8 caption. Colours follow Fig. 9.

1487 **Fig. 12.** Stratigraphic abundance versus last occurrence of the late Changhsingian foraminifer species from
1488 the Cili (A), Dajiang (B), Liangfengya (C), and Meishan (D) sections. Blue dots represent species with
1489 stratigraphic abundances > 15%. Pink boxes represent the number of species disappear or extinct within
1490 corresponding distance. Dajiang and Meishan are cited from [Song et al. \(2009b\)](#) and [Song et al. \(2009a\)](#),
1491 respectively.

1492 **Fig. 13.** Number of foraminifer species recorded from different (A) environments, (B) orders, and (C) types
1493 in South China from the late Changhsingian (*C. yini* Zone) to late Griesbachian. Shallow-water dwellers are
1494 mainly seen on the platforms but occasionally recognized in the slope facies. Widespread species are occurred
1495 in all three facies.

1496 **Fig. 14.** The deep-ward migration of foraminifers during the PTME. Sea surface temperature data is from
1497 [Joachimski et al. \(2012\)](#) and [Sun et al. \(2012\)](#). Red lines and grey shadows represent the mean sea surface
1498 temperature and 95% confidence intervals in the three time bins. Volcanism events are from [Burgess et al.](#)
1499 [\(2017\)](#) and [Yin and Song \(2013\)](#). Section abbreviations as in Fig. 8 caption; SST = sea surface temperature.

1500 **Fig. 15.** The spatial and temporal distribution of (A) shallow-water and (B) widespread foraminiferal species
1501 during the Permian-Triassic transition. Abbreviations consistent with Fig. 14

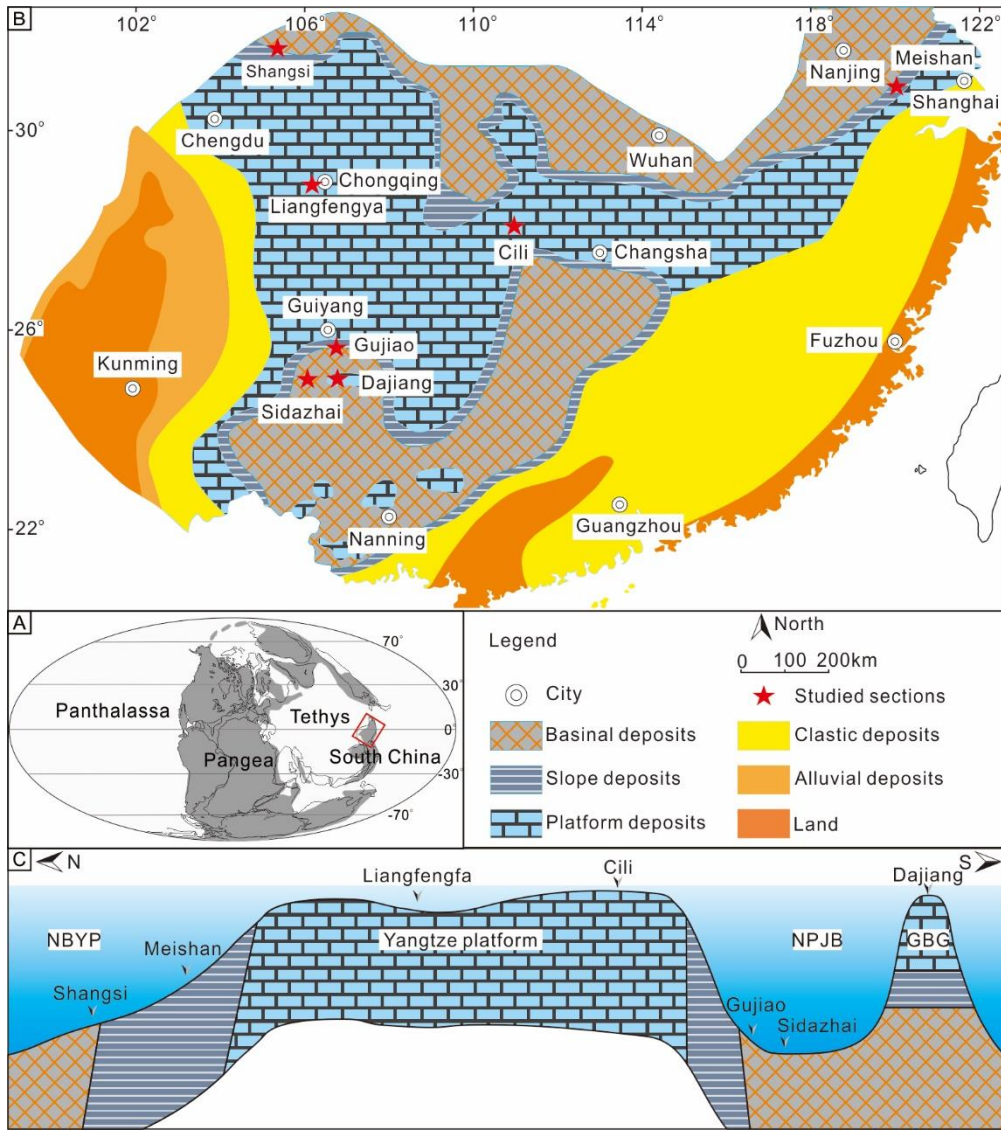
1502 **Fig. 16.** Sample-based rarefaction curves for the late Changhsingian, the PTB interval, and the late

1503 Griesbachian intervals. The dashed lines represent 95% confidence intervals.

1504 **Fig. 17.** Sample-based rarefaction curves for platform, slope, and basinal environments. (A) Rarefaction
1505 curves in the *C. yini* Zone. (B) Rarefaction curves in the PTB interval. (C) Rarefaction curves in the late
1506 Griesbachian. The black lines represent curves from the platform environment. The blue lines represent
1507 curves from slope environment. The blue-violet represent curves from the basin environment. The dashed
1508 lines represent 95% confidence intervals.

1509

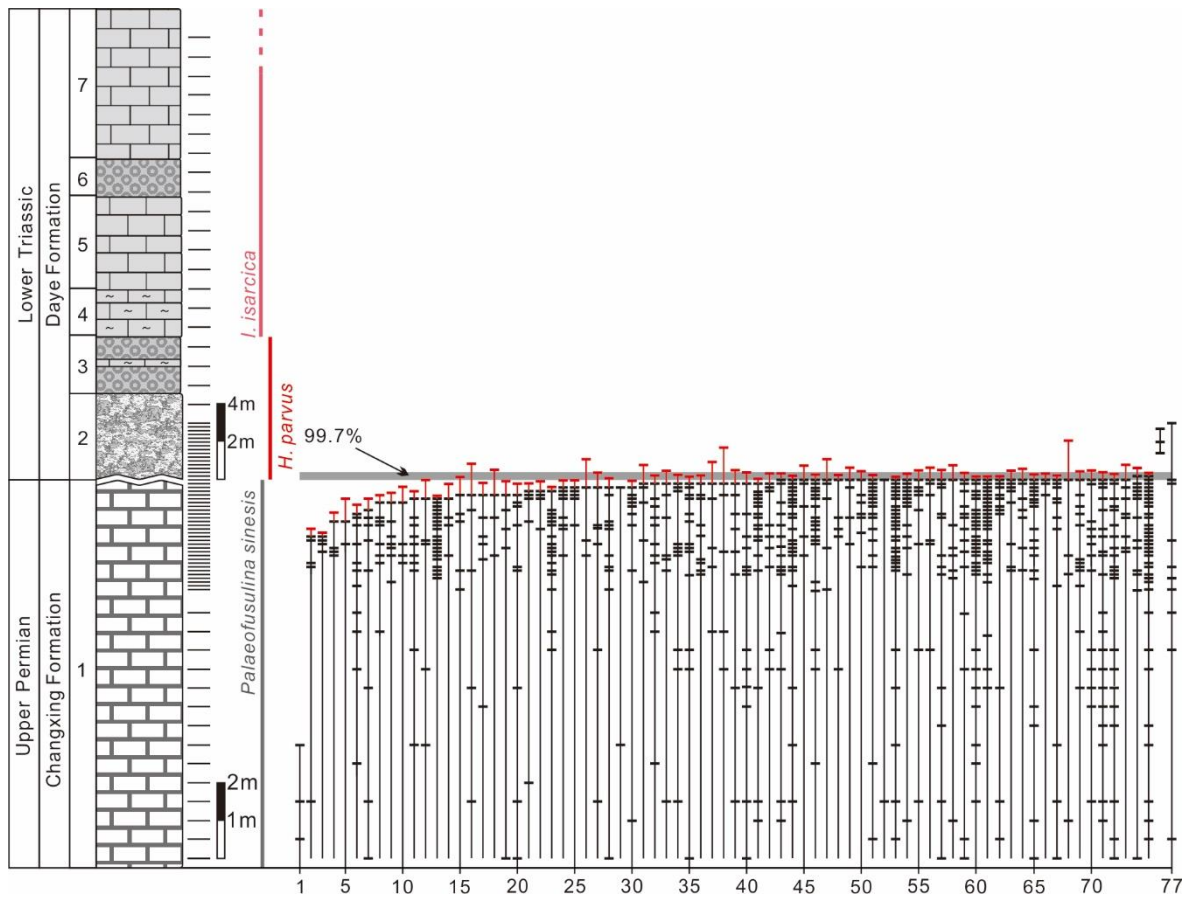
1510 **Table 1** Species diversity distribution of the main foraminifer groups in each section in the *C. yini* Zone, PTB
1511 interval, and late Griesbachian.



1512

1513

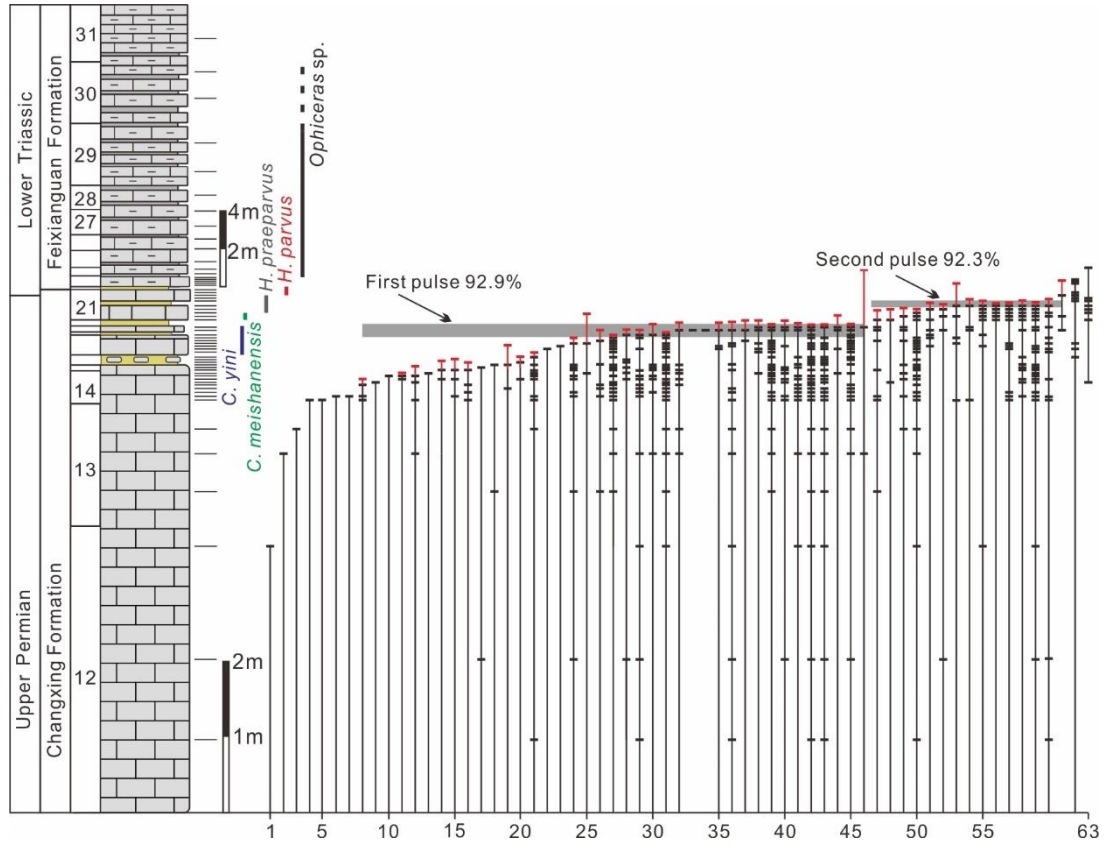
Fig. 1



1516

1517

Fig. 3



1518

1519

Fig. 4

1520

1521

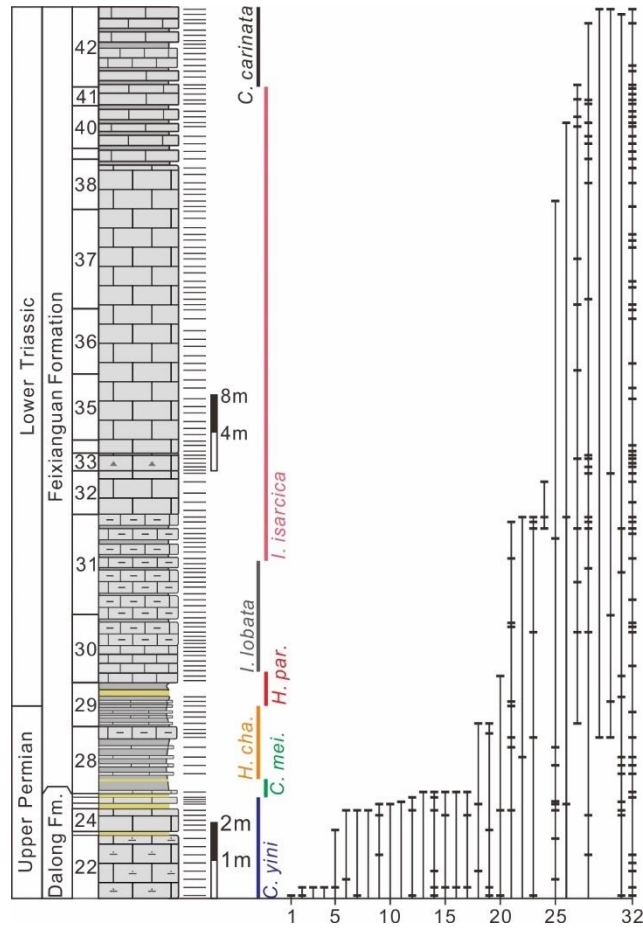
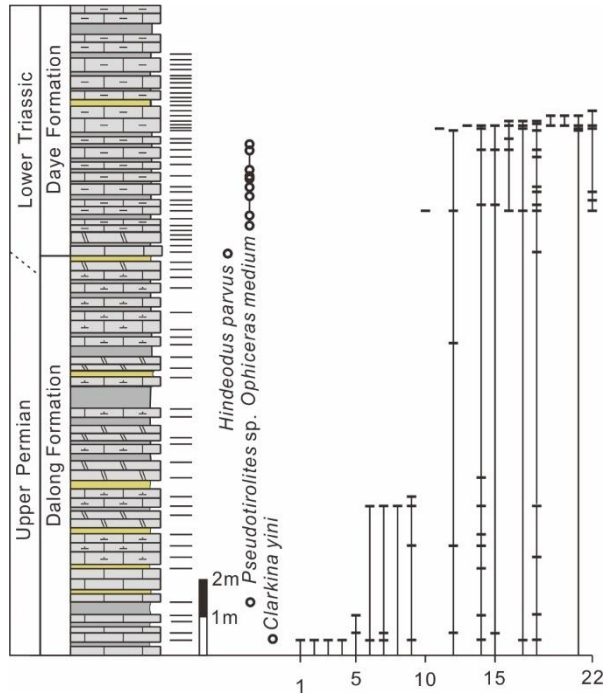


Fig. 5



1522

1523

Fig. 6

1524

1525

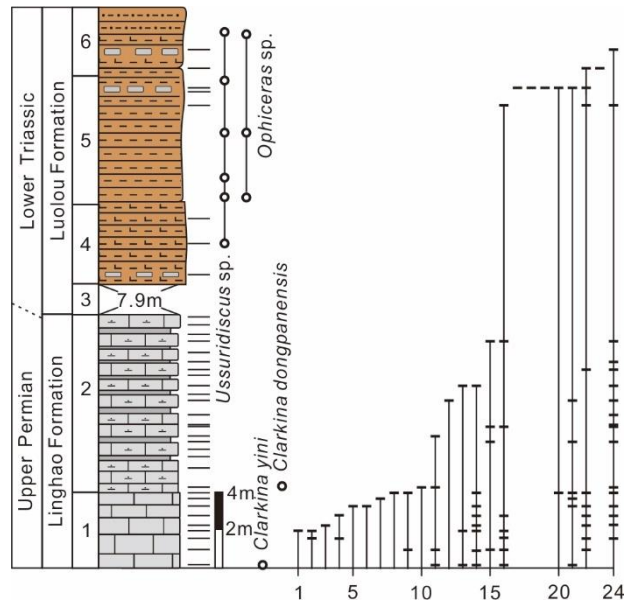
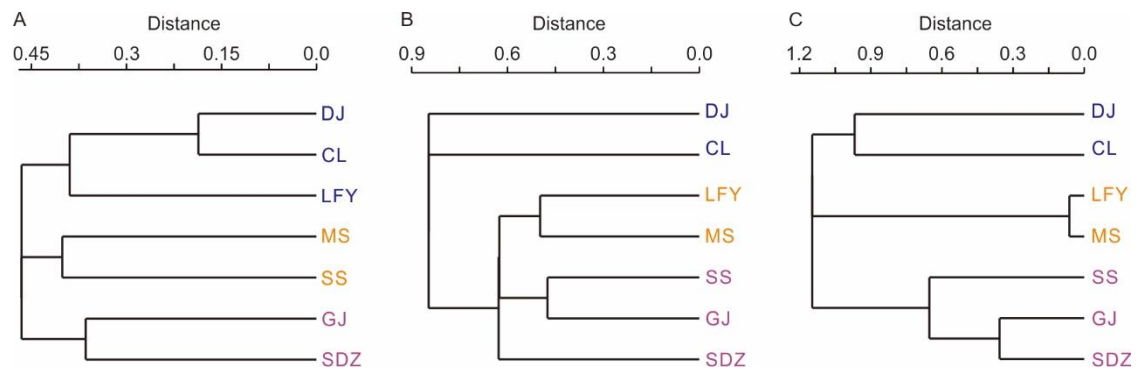


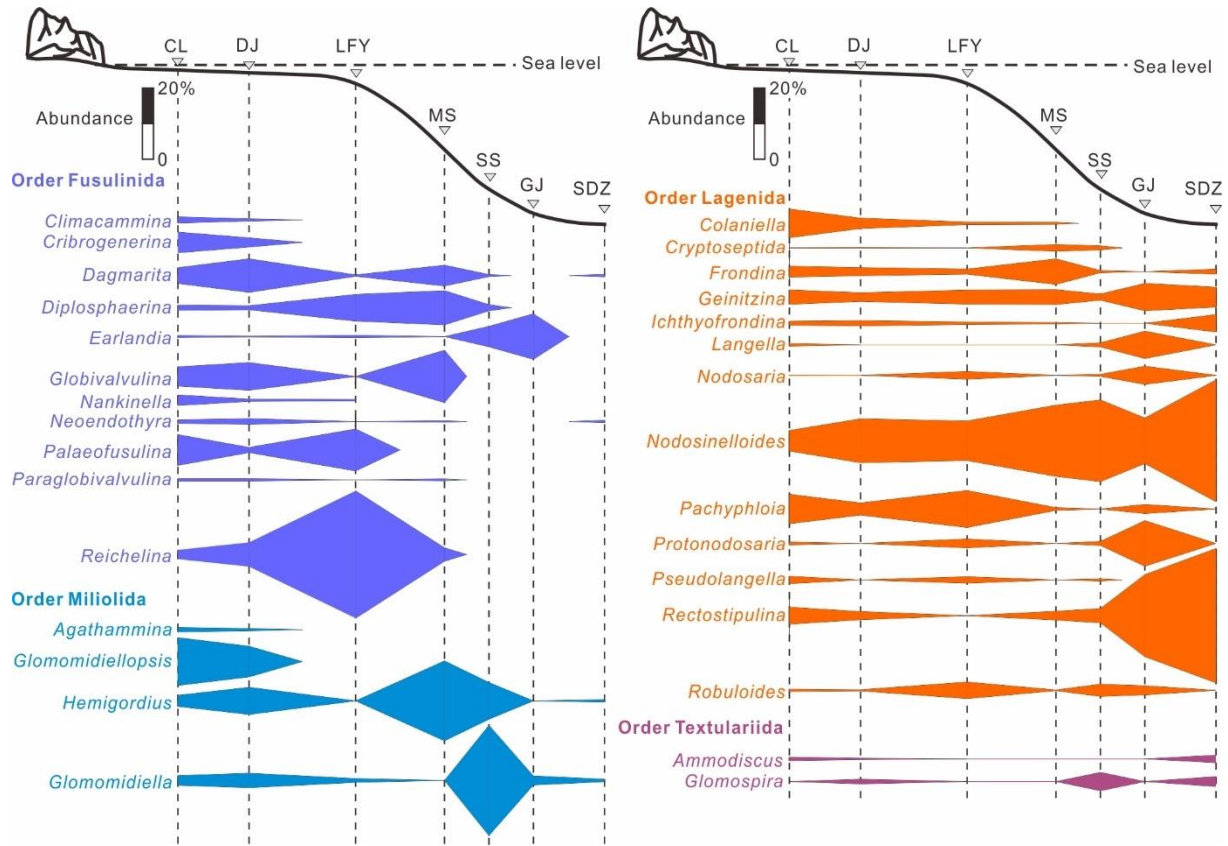
Fig. 7



1526

1527

Fig. 8



1528

1529

Fig. 9

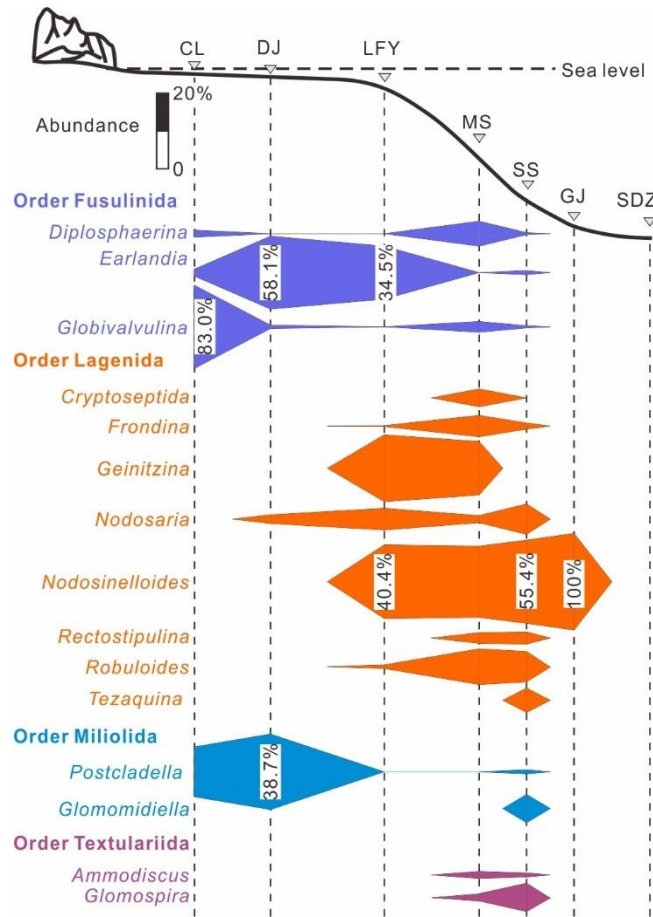
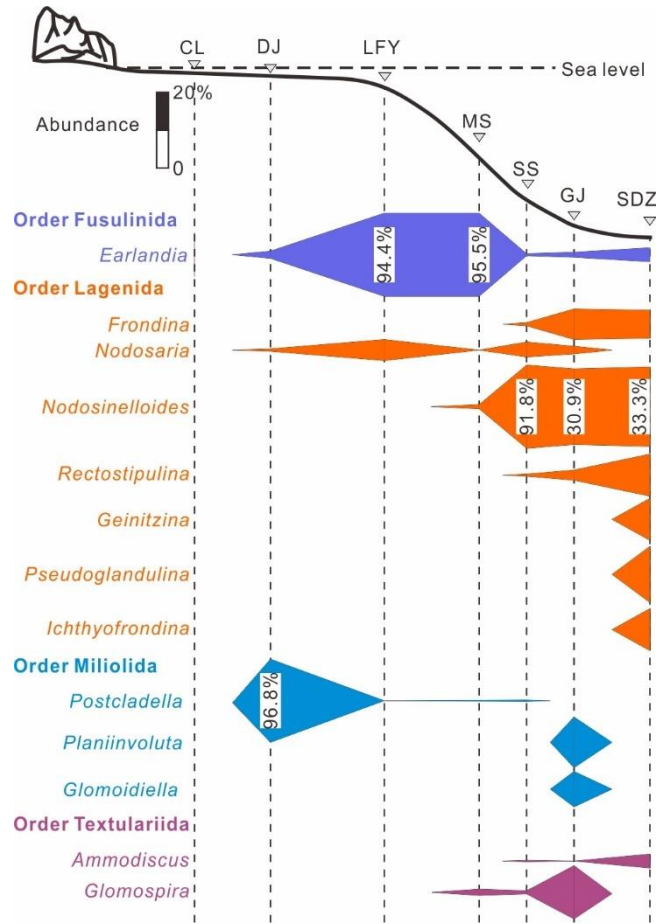


Fig. 10

1530

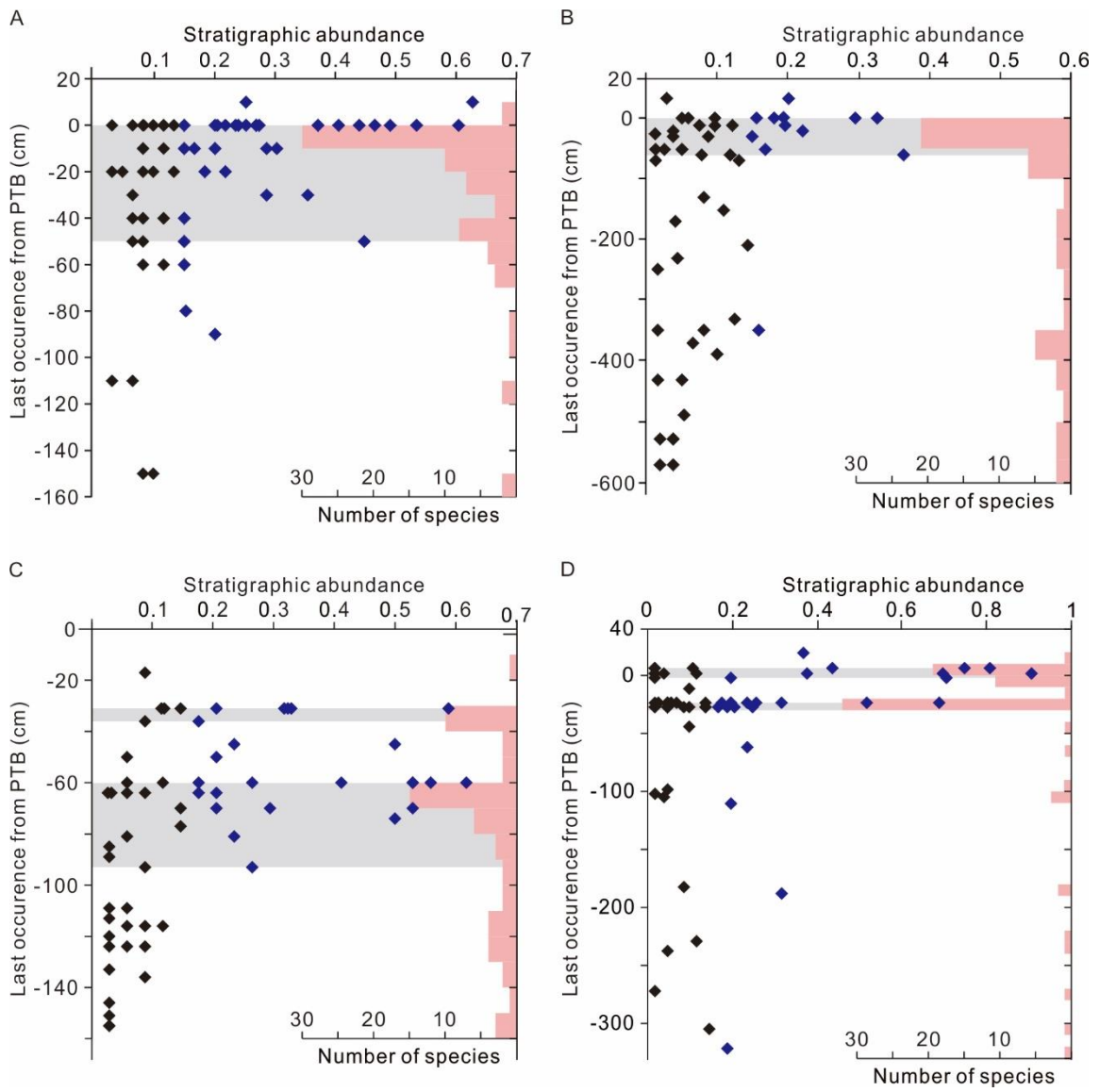
1531



1532

1533

Fig. 11

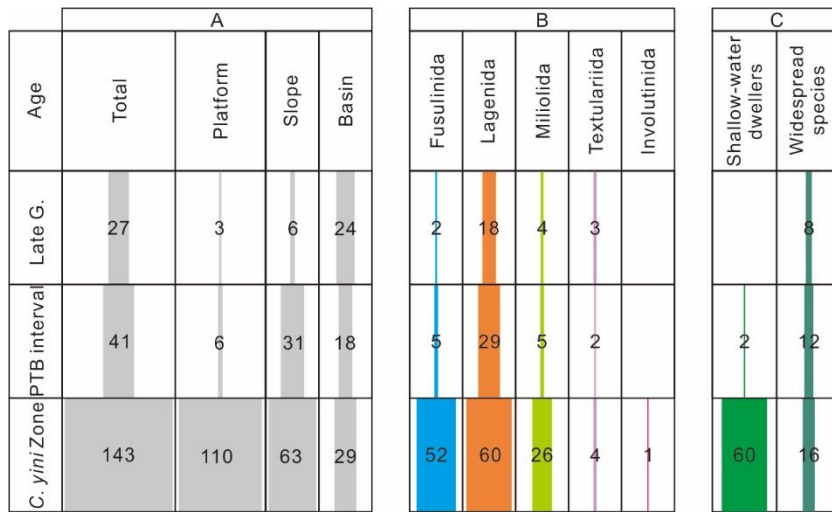


1534

1535

Fig. 12

1536



1537

1538

Fig. 13

1539

1540

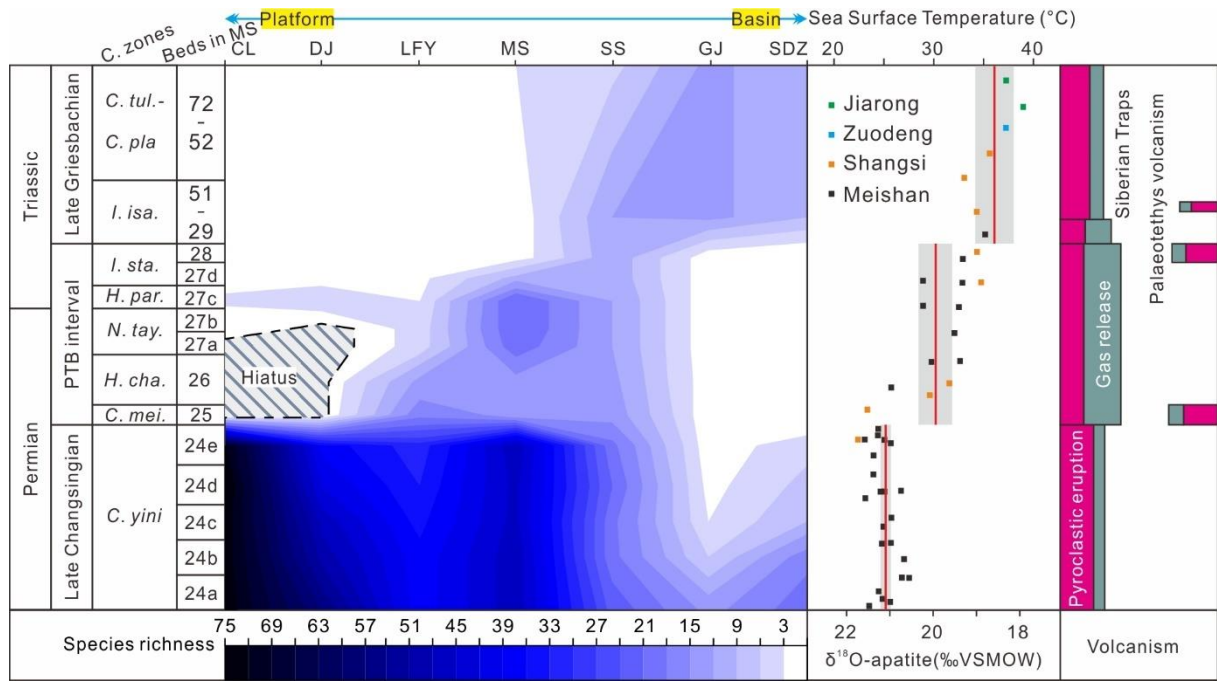
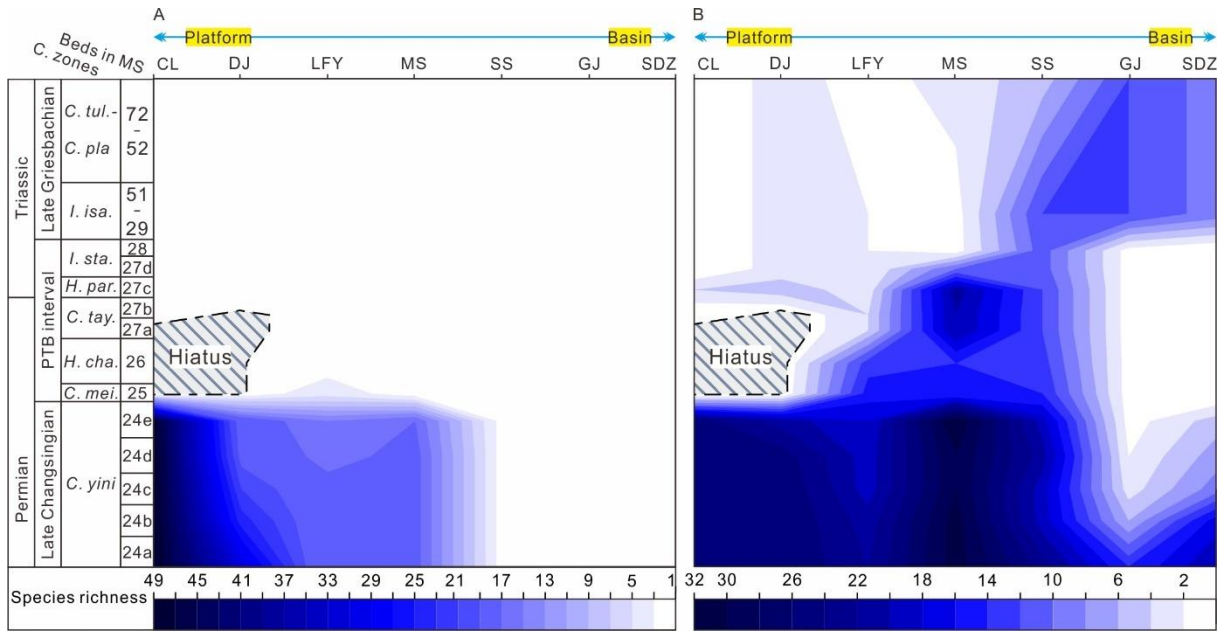


Fig. 14



1541

1542

Fig. 15

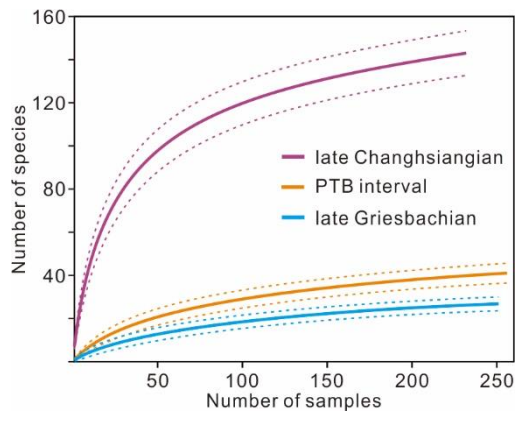


Fig. 16

1543

1544

1545

1546

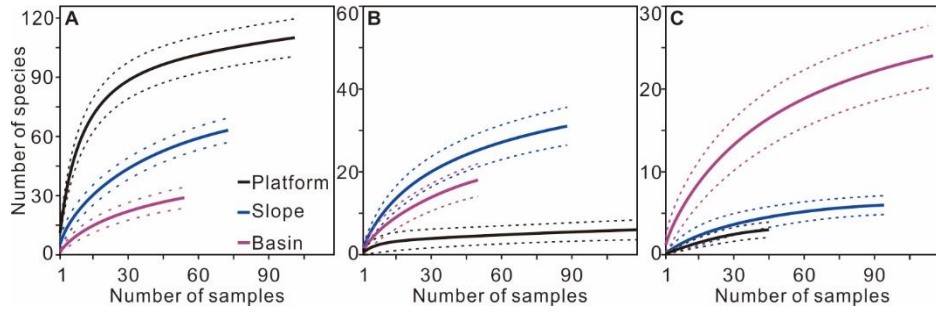


Fig. 17

Age	Order	Cili	Dajiang	Liangfengya	Meishan	Shangsi	Gujiao	Sidazhai
Late Griesbachian	Fusulinda	0	1	1	1	1	2	1
	Lagenida	0	1	1	2	8	8	7
	Miliolida	0	1	0	0	1	2	0
	Textulariida	0	0	0	2	2	1	1
PTB interval	Fusulinda	3	2	1	4	3	0	0
	Lagenida	0	1	15	15	10	1	0
	Miliolida	1	2	0	2	3	0	0
	Textulariida	0	0	0	2	2	0	0
C. yini Zone	Fusulinda	29	26	15	13	3	1	2
	Lagenida	32	24	22	24	14	10	14
	Miliolida	10	7	2	9	8	2	2
	Textulariida	1	2	0	2	1	0	2
	Involutinida	0	1	0	0	0	1	0

1547

1548

1549

Table 1